A chronologically reliable record of 17,000 years of biomass burning in the Lake Victoria area

Yunuen Temoltzin-Loranca, Erika Gobet, Boris Vannière, Jacqueline F N van Leeuwen, Giulia Wienhues, Sönke Szidat, Colin Courtney-Mustaphi, Mary Kishe, Moritz Muschick, Ole Seehausen, et al.

Quaternary Science Reviews 301 (2023) 107915

Contents lists available at ScienceDirect

Quaternary Science Reviews

journal homepage: www.elsevier.com/locate/quascirev

A chronologically reliable record of 17,000 years of biomass burning in the Lake Victoria area

Yunuen Temoltzin-Loranca [a, b, *], Erika Gobet [b], Boris Vannière [b, c], Jacqueline F.N. van Leeuwen [b], Giulia Wienhues [a], Sönke Szidat [d], Colin Courtney-Mustaphi [e], Mary Kishe [f], Moritz Muschick [g, h], Ole Seehausen [g, h], Martin Grosjean [a], Willy Tinner [b]

[a] Institute of Geography and Oeschger Center for Climate Change Research, University of Bern, Bern, Switzerland
[b] Institute of Plant Sciences and Oeschger Center for Climate Change Research, University of Bern, Bern, Switzerland
[c] Chrono-environnement, MSHE, CNRS, Université Bourgogne Franche Comté, Besançon, France
[d] Department of Chemistry, Biochemistry and Pharmaceutical Sciences and Oeschger Center for Climate Change Research, University of Bern, Bern, Switzerland
[e] Department of Environmental Sciences, Geoecology, University of Basel, Basel, Switzerland
[f] Tanzania Fisheries Research Institute, Dar es Salaam, Tanzania
[g] Department of Fish Ecology and Evolution, Center for Ecology, Evolution, and Biogeochemistry, Swiss Federal Institute for Aquatic Science and Technology (EAWAG), Kastanienbaum, Switzerland
[h] Aquatic Ecology and Evolution, Institute of Ecology and Evolution, University of Bern, Bern, Switzerland

ARTICLE INFO

Article history:
Received 30 June 2022
Received in revised form
8 December 2022
Accepted 11 December 2022
Available online 28 December 2022

Handling Editor: Giovanni Zanchetta

Keywords:
Fire
Charcoal
Chronology
Radiocarbon
Late Pleistocene
Holocene
Pollen
Lake Victoria

ABSTRACT

Fire regimes differ across tropical and subtropical biomes depending on multiple parameters whose interactions and levels of importance are poorly understood, particularly at multidecadal and longer time scales. In the catchment of Lake Victoria, savanna, rainforest, and Afromontane vegetation have interspersed over the last 17,000 years, which may have influenced the fire regime and vice versa. However, climate and humans are most often the primary drivers of fire regime changes, and analysing their respective roles is critical for understanding current and future fire regimes. Besides a handful of radiocarbon dates on grassy charcoal, the timescales of published studies of Lake Victoria sediment chronologies rely mostly on dates of bulk sediment, and chronological disagreements persist, mainly due to variation between estimations of the ^{14}C reservoir effect. Here, we provide independent ^{14}C chronologies for three Late Glacial and Holocene lacustrine sediment cores from various water depths and compare them with the biostratigraphy to establish a new chronological framework. We present the first continuous sedimentary charcoal records from Lake Victoria; these suggest that fire activity varied substantially during the past 17,000 years. Our new pollen records reveal the long-term vegetation dynamics. The available evidence suggests that before human impact increased during the Iron Age (ca. 2400 yr BP), biomass burning was linked to climate and vegetation reorganizations, such as warming, drying, and the expansion of rainforests and savannas. Our results imply that climate can trigger substantial fire regime changes and that vegetation responses to climate change can co-determine the fire regime. For instance, biomass burning decreased significantly when the rainforest expanded in response to increasing temperatures and moisture availability. Such insights into the long-term linkages between climate, vegetation, and the fire regime may help to refine ecosystem management and conservation strategies in a changing global climate.

1. Introduction

The Late Pleistocene and Holocene chronology of Lake Victoria's palaeoenvironmental history has been widely discussed but remains uncertain (Kendall, 1969; Beuning, 1999; Stager and Johnson,

* Corresponding author. Institute of Geography, Institute of Plant Sciences, and Oeschger Center for Climate Change Research, University of Bern, Bern, Switzerland.
E-mail address: yunuen.temoltzin@giub.unibe.ch (Y. Temoltzin-Loranca).

https://doi.org/10.1016/j.quascirev.2022.107915

2000; Talbot and Lærdal, 2000; Beuning et al., 2002). The timescales of published studies of Lake Victoria since the lake refilled with water during the Late Pleistocene rely on sediment cores that were predominantly bulk dated with only a couple of radiocarbon dates. The age–depth relationship has been modelled with a range of ^{14}C reservoir effect estimates (e.g. Beuning et al., 1997; Kendall, 1969; Stager et al., 1997). Although early studies extended to the Late Glacial period, more recent studies have not gone beyond the Holocene (Nakintu and Lejju, 2016; Andama, 2012). However, substantial chronological uncertainty and disparity exists between these records, which makes it difficult to compare the available palaeo time series both across East Africa and within the lake. This chronological issue represents a challenge when seeking to compare the signals of different proxies, for instance fire and vegetation responses to large-scale events such as Heinrich Event 1 and the African Humid Period and to local processes such as the desiccation of Lake Victoria (Stager et al., 2011; Garcin et al., 2007).

The long-term linkages between climate, fire regimes, and vegetation have been explored in eastern Africa for the Younger Dryas period (e.g. Garcin et al., 2007; Githumbi, 2017). Some studies emphasized how biomass burning regimes were strongly influenced by climatic and vegetation changes, largely depending on biomass acting as fuel and moisture availability as fire inhibitor or facilitator (Colombaroli et al., 2014; Nelson et al., 2012; Thevenon et al., 2003). Similar linkages have been observed in other regions of the world such as the Americas and Asia (e.g. Behling, 2002; Burbridge et al., 2004; Whitlock et al., 2010; Zhao and Yu, 2012).

Assessing the causes of fire regime shifts is important because burning modulates the structure, composition, productivity, and diversity of vegetation. It may also create positive or negative feedbacks via fuel availability and flammability, for instance if more or less flammable species are promoted by disturbance (e.g. Henne et al., 2015; Pedrotta et al., 2021). Moreover, the diverse properties of the three major vegetation types around Lake Victoria, the savanna, the rain forest and the Afromontane, may have significantly affected the fire regimes (e.g. Beuning, 1999; Kendall, 1969).

Due to the lack of continuous Holocene fire reconstructions for the Lake Victoria basin, the extent to which fires were controlled by climate, biomass change, and human impact remains unknown. This gap in information reduces our ability to understand the processes and mechanisms which controlled past fire regimes in the Lake Victoria basin. Such information is lacking for many regions of equatorial eastern Africa (Githumbi, 2017). However, the few studies which are available suggest that biomass burning increased in response to regional drought phases at Lake Albert, Mount Kenya, and Mount Kilimanjaro during Heinrich Event 1 (Beuning et al., 1997; Rucina et al., 2009; Schüler et al., 2012).

This study has three aims. The first is to provide a novel chronology for three new sediment cores from Lake Victoria based predominantly on macroscopic charcoal (>200 μm). The established chronology is validated for internal coherence by the biostratigraphy of our three cores. The second is to present the first continuous macroscopic charcoal analysis to reconstruct Late Glacial and Holocene fire history. The third is to discuss the long-term linkages between climate, fire, and vegetation in the Lake Victoria area.

2. Material and methods

2.1. Study site

Lake Victoria is located in East Africa at an altitude of 1135 m above sea level (m a.s.l). Overall, the rainfall regime in the catchment has two rainy and two dry seasons per year. Mean present-day annual precipitation ranges from 1000 to 1500 mm. It is mainly controlled by the migration of the Intertropical Convergence Zone and of the African monsoons and the variability in the eastward-westward position of the Congo Air Boundary (CAB), and it is locally modified by orography and local albedos (Beverly et al., 2020; Colombaroli et al., 2018; Marchant et al., 2007; Nicholson, 2018; Okungu et al., 2005). At the lake's elevation, the mean annual temperature varies between 24 and 25 °C, while in the highlands at 1950 m a.s.l, it ranges around 14.3 °C and at 3250 m a.s.l. around 7.1 °C. Thus, the mean lapse rate is ca. 0.5 °C/100 m, but this varies across the altitudinal gradient and through geological time (Loomis et al., 2017). Monthly temperatures vary slightly throughout the year, resulting in a tropical climate (Duane et al., 2008).

In the Lake Victoria basin, the strong moisture gradient results in various tropical climates, that span from equatorial climate (Af) to monsoon climate (Am) and savanna climate (Aw) according to Köppen's classification (Köppen, 1936). Along this moisture gradient, the associated biomes develop: the rain forests and the wooded savannas with Af climate and the grassy savannas with Aw climate. Under cooler and more humid conditions and higher elevations, the area hosts Afromontane vegetation: subtropical and temperate climates (Cwb) according to Köppen. The lake extends into Tanzania, Kenya, and Uganda, and the lake basin gathers distinct vegetation types: Guineo–Congolian rainforest, transitional rainforest, swamp forest, scrub forest, riverine forest, Afromontane rainforest, Afromontane undifferentiated forest, evergreen and semi–evergreen bushland, and thicket and derived communities (White, 1983).

2.2. Sediment cores, chronology, and macrocharcoal

In October 2018, a field campaign organized by the University of Bern in collaboration with the Tanzania Fisheries Research Institute (TAFIRI) recovered sediment cores from four locations along a transect near the Shirati Bay (Fig. 1). The coring was performed with the UWITEC Niederreiter coring system of the Institute of Plant Sciences at University of Bern, which was adapted to reach seaworthy conditions with the aid of eight pontoons made of aluminium instead of rubber and special sea anchors. This paper relies on data from three cores (Fig. 1 a, b): Core LVC18_S1 (hereafter LV1) located at 01°06,914′ S, 33°55,146′ E at a water column depth of 37 m; core LVC18_S2 (LV2) located at 01°07,850′ S, 33°56,780′ E at a water column depth of 22.6 m; and core LVC18_S4 (LV4) located at 01°02,966′ S, 33°47,768' E at a water column depth of 63 m.

The amount of sediment was limited, and its use had to be optimized for as many analyses as possible, leading us to modify the charcoal extraction (see Appendix A), and avoid the usage of chemical products as proposed in some standard methods (Millspaugh and Whitlock, 1995; Mooney and Tinner, 2011). For the sieved charcoal analysis, a total of 1151 sediment samples (361 from LV1, 401 from LV2, and 389 from LV4) of ca. 9 cm^3 were taken continuously at 2 cm intervals and passed through a graded series of screens of mesh size 200, 100, 50, and 20 μm. Samples containing particles >200 μm were analysed under a stereoscopic microscope LEICA M125 at 50 × magnification to separate, measure, and count the charcoal particles and to screen for plant and animal macrofossils.

Charcoal particles were standardized as number of particles per cm^{-3}, and the sedimentation rate (cm/yr) was extracted from the age–depth model with Long et al.'s (1998) technique. These were then multiplied to calculate the charcoal influx or *ch*arcoal *a*ccumulation *r*ate (CHAR; number of particles cm^{-2} yr^{-1}). Given that in large water bodies charcoal particles can reach similar distances to those of pollen grains (Genet et al., 2021), and due to the lack of

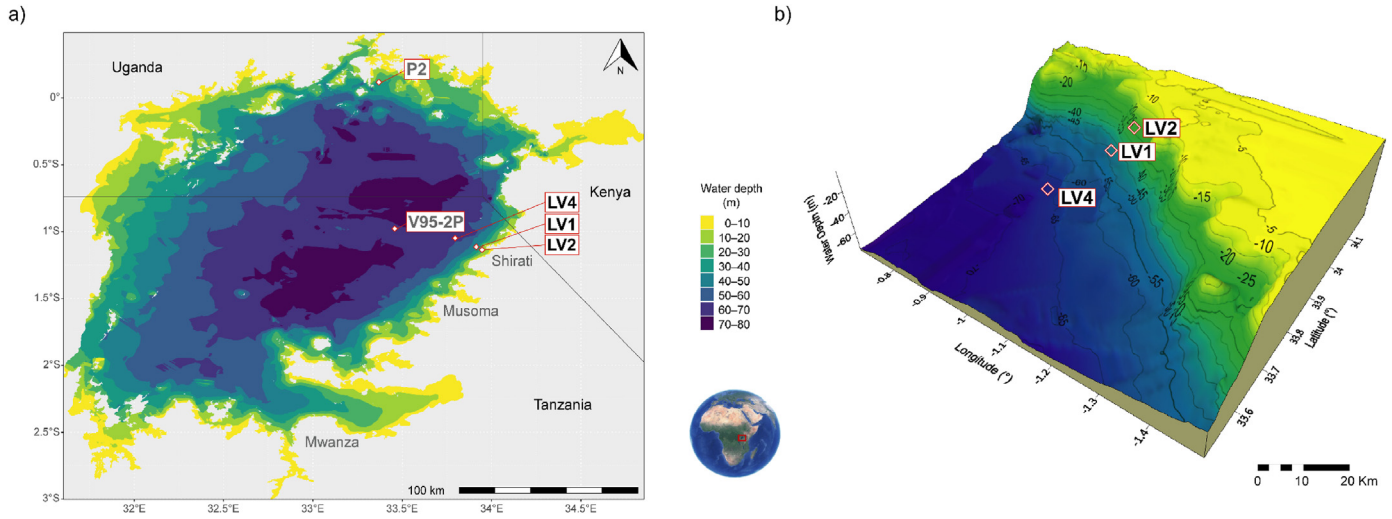

Fig. 1. (a) Bathymetry of Lake Victoria indicating the location of the new cores LV1, LV2, and LV4, and previously published cores: P2 (Kendall, 1969) and V95–2P (Beuning, 1999). Colour chart shows the water depth as of 2017. (b) Relief map of the lake floor according to water depth of 2017. Datapoints for elaborating both maps were extracted from Hamilton et al. (2016)

>0.6 mm particles, the fire signal was taken as regional (Adolf et al., 2018). The charred plant macroremains were separated, dried in the oven at 80 °C, and weighed. Subsequently, samples >0.10 mg were selected for AMS radiocarbon dating, which corresponded to 8% of the total samples.

In all three cores, the top of the composite was taken as the surface, and a total of 93 samples were radiocarbon dated. This was done with the MICADAS accelerator mass spectrometry (AMS) system at the Laboratory for the Analysis of Radiocarbon with AMS (LARA) at the University of Bern (Szidat et al., 2014) using two different approaches (Table 1). First, 31 samples of the 20–50 μm sieved fraction (containing all organic structures resistant to decay; from now on referred to as '20–50 μm palynomorph concentrate') representing all sites were treated for 3 h with 0.5 mol/L

Table 1
Radiocarbon dates of the Lake Victoria cores LV1 (LVC18_S1), LV2 (LVC18_S2) and LV4 (LVC18_S4) drilled in 2018.

Sample #	Laboratory code	Core	Sample ID	Composite core depth (cm)	Material	Carbon mass (μg)	^{14}C age (yr BP)*	Age corrected for ^{14}C reservoir effect for B and P (yr BP)*	Median ages (cal yr BP)	95 % C.I. (cal yr BP)	Model ages (cal yr BP)	Model age C.I.
1[1]	BE-13429	LVC18_S1	B1_20–22	022–024	C	12	−705 ± 170**	–	–	–	17	−63 −201
2[1]	BE-13430	LVC18_S1	B1_24–26	026–028	C	14	−225 ± 150***	–	–	–	51	−51 −260
3	BE-14379	LVC18_S1	B2_74–76	150–152	P	997	2250 ± 20	1680 ± 410	1635	751 −2695	1540	1137 −2070
4	BE-13425	LVC18_S1	B2_80–84	156–160	C	9	1410 ± 270	–	1317	743 −1872	1633	1212 −2227
5	BE-14384	LVC18_S1	B2_80–84	156–160	B	989	2300 ± 20	1730 ± 410	1689	828 −2705	1633	1212 −2227
6	BE-13418	LVC18_S1	B2_94–96	170–172	C	6	MEASUREMENT FAILED					
7	BE-15530	LVC18_S1	B3_70–72	246–248	P	989	3550 ± 30	2980 ± 410	3156	2120 −4159	3327	2801 −3737
8	BE-13420	LVC18_S1	C2_04–06	270–272	C	39	3540 ± 90	–	3826	3575 −4084	3736	3401 −3995
9	BE-14362	LVC18_S1	C2_30–32	296–298	C	52	3922 ± 100	–	4351	4003 −4795	3996	3627 −4301
10	BE-13416	LVC18_S1	C2_32–38	298–302	C	29	2780 ± 140	–	2920	2499 −3334	4016	3635 −4339
11	BE-15532	LVC18_S1	C2_34–36	300–302	P	994	4210 ± 30	3630 ± 410	3989	2883 −5044	4023	3641 −4339
12	BE-12182	LVC18_S1	B4_06–08	308–310	C	5	MEASUREMENT FAILED					
13	BE-13423	LVC18_S1	B4_18–20	322–324	C	9	2960 ± 300	–	3128	2358 −3833	4183	3791 −4531
14	BE-15533	LVC18_S1	B4_22–24	326–328	P	985	4380 ± 30	3800 ± 410	4208	3177 −5315	4221	3833 −4574
15	BE-13422	LVC18_S1	B4_26–28	330–332	C	8	3250 ± 320	–	3488	2745 −4394	4263	3867 −4621
16	BE-15534	LVC18_S1	B4_46–48	350–352	P	985	4680 ± 30	4100 ± 410	4596	3494 −5596	4475	4082 −4892
17	BE-15535	LVC18_S1	B4_72–74	376–378	P	990	5060 ± 30	4480 ± 410	5081	3980 −6168	4767	4367 −5274

(*continued on next page*)

Table 1 (*continued*)

Sample #	Laboratory code	Core	Sample ID	Composite core depth (cm)	Material	Carbon mass (μg)	^{14}C age (yr BP)*	Age corrected for ^{14}C reservoir effect for B and P (yr BP)*	Median ages (cal yr BP)	95 % C.I. (cal yr BP)	Model ages (cal yr BP)	Model age C.I.
18	BE-13421	LVC18_S1	B4_74–76	378–380	C	14	3980 ± 200	–	4439	3876 –4691	4790	4381 –5318
19	BE-15536	LVC18_S1	B5_09–11	402–404	P	990	5220 ± 30	4640 ± 410	5276	4242 –6220	5209	4746 –5764
20	BE-13424	LVC18_S1	B5_17–19	410–412	C	11	4390 ± 320	–	4989	4093 –5840	5374	4896 –5942
21	BE-13419	LVC18_S1	B5_39–41	432–434	C	3	MEASUREMENT FAILED					
22	BE-15537	LVC18_S1	B5_57–59	450–452	P	992	6200 ± 35	5630 ± 410	6443	5584 –7418	6382	5736 –7007
23	BE-15538	LVC18_S1	B5_83–85	476–478	P	987	6810 ± 35	6240 ± 410	7076	6214 –7928	7053	6408 –7625
24	BE-15531	LVC18_S1	B6_10–12	502–504	P	910	7380 ± 40	6810 ± 410	7663	6749 –8424	7603	6982 –8134
25	BE-15539	LVC18_S1	B6_36–38	528–530	P	996	7830 ± 40	7250 ± 410	8097	7312 –9017	8123	7614 –8618
26[2,3]	BE-14377	LVC18_S1	C5_01–03	546–548	C	18	13900 ± 430	–	16842	15681 –18091	–	–
27	BE-12183	LVC18_S1	C5_23–25	566–568	C	56	8430 ± 120	–	9409	9029 –9658	8920	8611 –9346
28	BE-13417	LVC18_S1	C5_21–23	566–568	C	30	7300 ± 130	–	8119	7867 –8376	8920	8611 –9346
29	BE-12184	LVC18_S1	C6_07–09	624–626	C	2	MEASUREMENT FAILED					
30	BE-12185	LVC18_S1	C6_11–13	628–630	C	51	9490 ± 120	–	10801	10437 –11182	10889	10392 –11328
31	BE-12186	LVC18_S1	C6_39–41	656–658	C	4	MEASUREMENT FAILED					
32	BE-12187	LVC18_S1	C6_51–53	668–670	C	14	10550 ± 370	–	12295	11254 –13114	12578	11939 –13091
33	BE-12189	LVC18_S1	C6_63–65	680–682	W	38	11500 ± 170	–	13375	13095 –13748	13140	12775 –13433
34	BE-12188	LVC18_S1	C6_63–65	680–682	C,W,X	14	10000 ± 370	–	11599	10574 –12689	13140	12775 –13433
35	BE-12190	LVC18_S1	C6_79–81	696–698	C	13	11900 ± 480	–	13961	12840 –15304	13414	13131 –13780
36	BE-12191	LVC18_S1	C6_81–83	698–700	S, C	53	11600 ± 160	–	13465	13173 –13781	13449	13157 –13849
37	BE-12192	LVC18_S1	C6_89–91	706–708	W	3	MEASUREMENT FAILED					
38	BE-12193	LVC18_S1	C6_89–91	706–708	C	2	MEASUREMENT FAILED					
39	BE-15540	LVC18_S2	E2_34–36	126–128	P	920	1800 ± 30	1230 ± 410	1163	335 –2094	1210	748 –1748
40	BE-15541	LVC18_S2	E2_60–62	154–156	P	900	1980 ± 30	1410 ± 410	1343	557 –2302	1500	1014 –2065
41	BE-15542	LVC18_S2	E2_90–92	184–186	P	868	2260 ± 30	1690 ± 410	1646	787 –2696	1848	1384 –2405
42	BE-15543	LVC18_S2	E3_18 ––20	212–214	P	834	2620 ± 30	2050 ± 410	2043	1129 –2998	2251	1739 –2843
43	BE-15544	LVC18_S2	E3_46–48	240–242	P	718	2870 ± 40	2300 ± 410	2327	1396 –3329	2692	2112 –3381
44	BE-15545	LVC18_S2	F4_15–17	268–270	P	972	3310 ± 30	2740 ± 410	2860	1828 –3848	3289	2619 –4001
45	BE-14367	LVC18_S2	F4_67–73	320–326	C,R	37	4160 ± 100	–	4679	4416 –4953	4705	4201 –5062
46	BE-13426	LVC18_S2	F5_72–73	403–404	L	997	5360 ± 20	–	6144	6007 –6273	6120	6006 –6265
47	BE-14370	LVC18_S2	E5_80–82	432–434	C	92	5470 ± 80	–	6259	6004 –6436	6378	6202 –6679
48	BE-14372	LVC18_S2	E6_08–16	458–466	C	32	6170 ± 120	–	7054	6747 –7318	7055	6709 –7384
49	BE-14366	LVC18_S2	E6_16–20	466–470	C	28	6250 ± 140	–	7135	6796 –7426	7144	6831 –7461
50	BE-15546	LVC18_S2	F6_19–21	506–508	P	833	7280 ± 40	6710 ± 410	7560	6678 –8367	7807	7332 –8340
51	BE-14375	LVC18_S2	F7_33–35	550–552	C	46	7920 ± 110	–	8773	8455 –9022	8746	8418 –9110
52[2,3]	BE-14371	LVC18_S2	E7_34–38	588–592	C,W	21	7200 ± 180	–	8023	7688 –8360	–	–
53	BE-15547	LVC18_S2	E7_50–52	604–606	P	862	8780 ± 40	8200 ± 410	9129	8207 –10182	9609	9126 –10115
54	BE-14364	LVC18_S2	E8_21–31	628–638	C	45	9030 ± 130	–	10156	9715 –10503	10214	9818 –10432
55	BE-15548	LVC18_S2	E8_27–29	634–636	P	871	9180 ± 40	8610 ± 410	9657	8554 –10680	10249	10071 –10410
56	BE-13427	LVC18_S2	E8_34–35	641–642	T	987	9243 ± 20	–	10416	10292 –10504	10376	10262 –10480

Table 1 (*continued*)

Sample #	Laboratory code	Core	Sample ID	Composite core depth (cm)	Material	Carbon mass (μg)	^{14}C age (yr BP)*	Age corrected for ^{14}C reservoir effect for B and P (yr BP)*	Median ages (cal yr BP)	95 % C.I. (cal yr BP)	Model ages (cal yr BP)	Model age C.I.
57	BE-14369	LVC18_S2	E8_35–37	642–644	C	136	9320 ± 300	–	10569	9609 –11314	10391	10278 –10500
58	BE-13428	LVC18_S2	E8_37–38	644–645	T	987	9230 ± 20	–	10393	10282 –10499	10420	10306 –10527
59	BE-14374	LVC18_S2	E8_47–53	654–660	C	43	9110 ± 130	–	10288	9821 –10652	10561	10358 –11153
60	BE-15549	LVC18_S2	E8_55–57	662–664	P	964	10100 ± 50	9560± 410	10923	9697 –12434	10768	10507 –11284
61	BE-14373	LVC18_S2	E8_75–77	682–684	C	40	10300 ± 150	–	12099	11404 –12621	11798	10507 –11284
62	BE-14368	LVC18_S2	E8_77–87	684–694	C	106	10200 ± 110	–	11878	11397 –12466	11902	11387 –12387
63	BE-15550	LVC18_S2	E8_83–85	690–692	P	813	10500 ± 50	9970 ± 410	11554	10421 –12720	11936	11490 –12332
64	BE-14365	LVC18_S2	E9_07–15	714–722	C	37	10400 ± 160	–	12240	11653 –12723	12516	11986 –12980
65	BE-15551	LVC18_S2	E9_11–13	718–720	P	927	11200 ± 50	10630 ± 410	12379	11249 –13297	12537	12030 –12951
66	BE-15552	LVC18_S2	E9_39–41	746–748	P	823	11900 ± 50	11360 ± 410	13274	12108 –14308	13333	13022 –13689
67	BE-14376	LVC18_S2	E9_41–43	748–750	C	70	11500 ± 140	–	13372	13104 –13605	13413	13094 –13778
68	BE-14363	LVC18_S2	E9_93–95	800–802	C,W,S	99	13000 ± 130	–	15557	15189 –15944	15424	14405 –15923
69	BE-16248	LVC18_S4	L2_31–35	116–118	C	32	2890 ± 100	–	3035	2781 –3329	3051	2770 –3344
70	BE-16249	LVC18_S4	L2_59–63	144–148	C	71	3290 ± 70	–	3517	3373 –3690	3539	3293 –3787
71	BE-16262	LVC18_S4	L2_61–63	146–148	P	968	3400 ± 25	2830 ± 410	2972	1932 –3980	3557	3344 –3787
72	BE-16250	LVC18_S4	L2_85–87	170–172	C	105	3670 ± 70	–	4004	3777 –4233	4043	3832 –4268
73	BE-16251	LVC18_S4	L3_03–05	188–190	C	37	3990 ± 90	–	4463	4156 –4814	4404	4155 –4649
74	BE-16252	LVC18_S4	L3_23–27	208–212	C	47	4190 ± 90	–	4706	4440 –4959	4774	4488 –5151
75	BE-16263	LVC18_S4	L4_18–20	272–274	P	995	5770 ± 30	5200 ± 410	5952	4883 –6882	6273	5946 –6564
76	BE-16253	LVC18_S4	L4_18–22	272–276	C	43	5500 ± 100	–	6294	6003 –6492	6297	5946 –6647
77	BE-16254	LVC18_S4	L5_09–11	334–336	C	55	6570 ± 100	–	7468	7273 –7613	7498	7198 –7773
78	BE-16255	LVC18_S4	L5_61–65	386–390	C	48	7910 ± 120	–	8763	8429 –9023	8749	8413 –9081
79	BE-16256	LVC18_S4	L5_93–97	418–422	C	53	8340 ± 110	–	9323	9029 –9531	9296	8958 –9585
80	BE-16264	LVC18_S4	L5_95–97	420–422	P	999	8510 ± 30	7940 ± 410	8843	7935 –9883	9311	8978 –9585
81	BE-16257	LVC18_S4	L6_58–60	484–486	C	62	9270 ± 120	–	10459	10201 –10988	10325	9829 –10657
82	BE-16258	LVC18_S4	L7_06–08	516–518	C	18	9000 ± 260	–	10103	9481 –11058	10620	10167 –11084
83	BE-16259	LVC18_S4	L7_36–38	546–548	C	31	9320 ± 190	–	10557	9974 –11182	11056	10597 –11626
84	BE-16265	LVC18_S4	L7_36–38	546–548	P	775	10200 ± 60	9660 ± 410	11068	9914 –12476	11056	10597 –11626
85	BE-16260	LVC18_S4	L8_30–32	594–596	C	25	10600 ± 230	–	12453	11755 –13066	12263	11581 –12850
86	BE-16261	LVC18_S4	L8_84–86	648–650	C	33	11500 ± 200	–	13379	13000 –13795	13447	13034 –13906
87	BE-15553	LVC18_S4	L9_10–12	674–676	C	50	12200 ± 190	–	14234	13614 –14974	14097	13716 –14565
88	BE-16266	LVC18_S4	L9_10–12	674–676	P	688	13000 ± 70	12300 ± 410	14478	13414 –15667	14097	13716 –14565
89	BE-15554	LVC18_S4	L9_20–24	684–686	C	60	12300 ± 170	–	14408	13808 –15003	14299	13866 –14791
90	BE-15555	LVC18_S4	L9_40–42	704–706	C	38	12000 ± 210	–	13920	13434 –14828	14738	14108 –15298
91	BE-15556	LVC18_S4	L10_02–04	762–764	C	194	13700 ± 170	–	16588	16081 –17056	16386	15899 –16826
92	BE-15557	LVC18_S4	L10_12–14	772–774	C	193	13700 ± 160	–	16589	16121 –17045	16596	16106 –17046

(*continued on next page*)

Table 1 (*continued*)

Sample #	Laboratory code	Core	Sample ID	Composite core depth (cm)	Material	Carbon mass (μg)	^{14}C age (yr BP)*	Age corrected for ^{14}C reservoir effect for B and P (yr BP)*	Median ages (cal yr BP)	95 % C.I. (cal yr BP)	Model ages (cal yr BP)	Model age C.I.
93	BE-16267	LVC18_S4	L10_12−14	772−774	P	248	14100 ± 110	13500 ± 410	16282	15046 −17432	16596	16106 −17046
94[2]	BE-16564	LVC18_CCS	L10−core catcher	Below last segment core	P	989	17200 ± 46	16600 ± 410	20044	19018 −20970	–	–

*Dates rounded following Stuiver & Polach (1977). ** F ^{14}C = 1.092 ± 0.023.***F ^{14}C = 1.028 ± 0.019. [1]Samples containing bomb ^{14}C. [2]Sample not included in the age−depth models.[3] Outliers. B = Bulk, C = Charcoal, R = Terrestrial plant remains, L = Lakeshore plant root/stem (Poales), P = 20−50 μm palynomorph concentrate, S = Terrestrial seed (*Carex* spp.), T = Twig, W = Wood, X = Terrestrial seed coat, C.I. = Confidence Interval.

hydrochloric acid (HCl) at 40 °C. These pre-treated samples were then transformed into graphite targets with automated graphitization equipment (AGE) and measured with the MICADAS. Second, 63 samples of isolated macrocharcoal were purified with 0.5 mol/L HCl for 3 h at 40 °C, followed by 0.1 mol/L sodium hydroxide (NaOH) for 15 min at room temperature and another step of 0.5 mol/L HCl for 3 h at 40 °C. Because of their low dry weight after treatment (8−130 μgC with an average of 46 μgC), graphitization was replaced by combustion of the samples and direct injection of the resulting carbon dioxide (CO_2) into the gas ion source of the MICADAS (Salazar et al., 2015). Zander et al. (2020) showed that the quality of a lake sediment chronology may improve with the implementation of small-sized gas samples, even though their individual age uncertainties are typically higher than for medium-to large-sized samples from graphite targets. Nevertheless, seven samples failed analysis due to their insufficient dry weight after chemical treatment. In LV1, there were two duplicated samples at 566 and 680 cm respectively, and in order to get the best age estimation, each sample was combined with its pair (from now on referred to as 'pooled dates') with OxCal 4.3 (R_combine, Bronk Ramsey C., 1994, 1995, 2001).

To assess chronological biases due to the ^{14}C reservoir effect, we constructed two age-depth models for each site: first, exclusively with dates originating from the palynomorph-bulk concentrate, which also contained algae cells such as *Pediastrum* and *Botryococcus;* and second, with dates originating solely from macrocharcoal. Then, we measured paired samples, and we calculated (i) the difference in ages of same depths between the 20−50 μm palynomorph concentrate and the microcharcoal and (ii) the mean and standard deviation of the differences of all three sites. The corrected ages of the 20−50 μm palynomorph concentrate and the terrestrial macrofossil ages were used to construct a combined model with its 95% (2σ) probabilities using rbacon (Blaauw and Christen, 2011; Blaauw et al., 2021) in R software and the IntCal20 calibration curve (Reimer et al., 2020).

Subsequently, after developing the three independent chronologies, we used the biostratigraphy of each site to crosscheck the resulting ages. For instance, the bottom of the record was aligned with the population decrease of Amaranthaceae/Chenopodiaceae and an apparent regional appearance of *Acalypha* towards ca. 14,500 cal yr BP (see section 3.3). Furthermore, during the Late Glacial, *Olea* pollen increases at 14,000−13,000 cal yr BP in all three records. Similarly, at 10,500 cal yr BP, *Alchornea* and *Acalypha* pollen increases at all sites. Moreover, *Celtis* pollen increases at ca. 8000 cal yr BP at all sites. Finally, at ca. 4500 cal yr BP, arboreal taxa such *Celtis* and Moraceae declined, and Poaceae increased at all three sites, signifying an expansion of open land. Our biostratigraphic comparison suggests that the three radiocarbon-based age-depth models provide robust and spatially reproducible chronologies.

2.3. Pollen analysis

We took a total of 80 sediment samples of 1 cm^3 at sampling intervals of ca. 35 cm at each site: 27 from LV1, 27 from LV2, and 26 from LV4. *Lycopodium* tablets were added to the samples prior to chemical treatment (Stockmarr, 1971). Samples were treated with HCl, KOH, HF, and acetolysis, following the standard methods for pollen extraction (Moore et al., 1991). For slide preparation, the samples were stained with fuchsine and diluted with glycerine. Pollen grains were identified under a light microscope at 400 × magnification and using palynological keys and photo atlases (Gosling et al., 2013; Reille, 1992; Roubik and Moreno, 1991; Schüler and Hemp, 2016) with the aid of the Mount Kilimanjaro reference collection at the palynological laboratory of the University of Göttingen, Germany. Pollen sums along the record range from 217 to 545 pollen grains per sample (mean = 390 pollen grains, standard deviation = 80).

Lake Victoria is located at a crucial ecological junction of three main biomes: the savanna, the rainforest, and the Afromontane forest. In this study, the grouping of the species by biome was made according to the Flora of Tropical East Africa (1955−2012), and only selected taxa from each biome were considered. All rainforest types mentioned in section 2.1 were grouped in the rainforest category, and the two types of Afromontane forests under Afromontane, which have a more complex structure than the rainforests, require more precipitation, and start developing under cooler conditions at 1200−1300 m.a.s.l. (White, 1983). Taking into account these considerations, we included Moraceae, *Mussaenda*, *Macaranga*, *Alchornea*, and *Urera*-type in the rainforest category and *Celtis*, *Podocarpus*, *Juniperus*, *Olea* and *Allophylus* in the Afromontane category.

Accordingly, *Celtis* can develop starting from 300 up to 2000 m a.s.l and develops most strongly between 1000 and 1800 m a.s.l. (Schüler and Hemp, 2016). *Podocarpus* occurs at 900 m a.s.l. but is more abundant between 2500 and 3100 m a.s.l (Schüler and Hemp, 2016). *Juniperus* is part of the Afromontane undifferentiated forest. Interestingly, this ecosystem is very sensitive to drier conditions, in which it undergoes kaleidoscopic changes in structure, and after fires it is replaced by stands of single, dominant Afromontane species such as *Juniperus procera* or *Hagenia abyssinica*. These vegetational changes occur between 1250 and 2500 m a.s.l. (Kindt et al., 2015). *Olea* has its greatest abundances between 2000 and 2500 m a.s.l., even though some subspecies can also grow in riverine fringes at lower altitudes. Lastly, in the lowlands, the savanna vegetation includes Poaceae, Cyperaceae, *Cyperus*-type, *Cissampelos*, *Acalypha*, *Combretum*, and Amaranthaceae/Chenopodiaceae. The terrestrial and the pollen grains from aquatic *Cyperus* were summed in the Cyperaceae category.

2.4. Numerical methods

2.4.1. Statistical analyses

The number of charcoal particles was resampled on a regular time bin, every 40 years based on the average accumulation rate. Then, we compared the three cores with a nonparametric two-sample Mann–Whitney test and the distribution of the charcoal influx (CHAR), as shown in boxplots (Fig. 5f). For each CHAR time series, we used a generalized additive model (GAM) to model and identify zones of similar trends. Additionally, to assess the trend change and highlight the phases of high, medium, or low values of CHAR, for each site we conducted a Bayesian change point analysis with the bcp v 4.0.5 package in R (Erdman and Emerson, 2007). The results between sites showed slight variations, but this was expected because the age uncertainty varies between models. Therefore, we decided to use only the change points of LV4, because their age uncertainty is the smallest of the three cores included in this study.

2.4.2. Pollen zonation and ordination

To determine the local pollen assemblage zones (LPAZ), we used the optimal partitioning approach with minimum sum of squares and the broken stick model (Bennett, 1996; Birks and Gordon, 1985), and the subzones in zone 1 were based on visual criteria.

Then, we conducted a principal component analysis (PCA) using Canoco 5.10 (ter Braak and Šmilauer, 2018) to seek similarities in samples between sites and correlations with temperature records in the area and with our charcoal records. Because our response data are compositional and have a short length of the gradient (sd = 1.5), we applied a linear ordination method on the square-root-transformed pollen percentage data (ter Braak and Prentice, 1988). We grouped the samples and represented groups by colour according to their LPAZ and by figure according to their sites of origin (Fig. 11). This ordination method was also performed site by site.

3. Results and interpretation

3.1. Chronology

Of the three age–depth models constructed (Figs. 2–4), LV4 (the deepest site in the transect) turned out to have the most reliable chronology with the highest number of terrestrial dates and, thus, smaller uncertainties.

The calculated mean difference between the 20–50 palynomorph concentrate and the microcharcoal resulted in 573 years, which were taken as the ^{14}C reservoir effect value and subtracted from each one of the ^{14}C palynomorph-bulk dates to correct for too old dates (Olsson, 2009). The calculated standard deviation, sd = 410, was then taken as the uncertainty. The reservoir effect was taken as constant across the three cores because the calculations were based on measurements from all three.

Sedimentation rates are comparable in all cores (mean: LV1 = 0.07, LV2 = 0.06, LV4 = 0.05 cm/yr) with only minor variability (sd: LV1 = 0.04, LV2 = 0.02, LV4 = 0.01 cm/yr). However, there are two separate sedimentation periods in LV1 and LV2: the first from the start of the records up to ca. 5000–3000 cal yr BP with lower sedimentation rates and the second from then to the present with increased sedimentation rates (Figs. 2 and 3). The

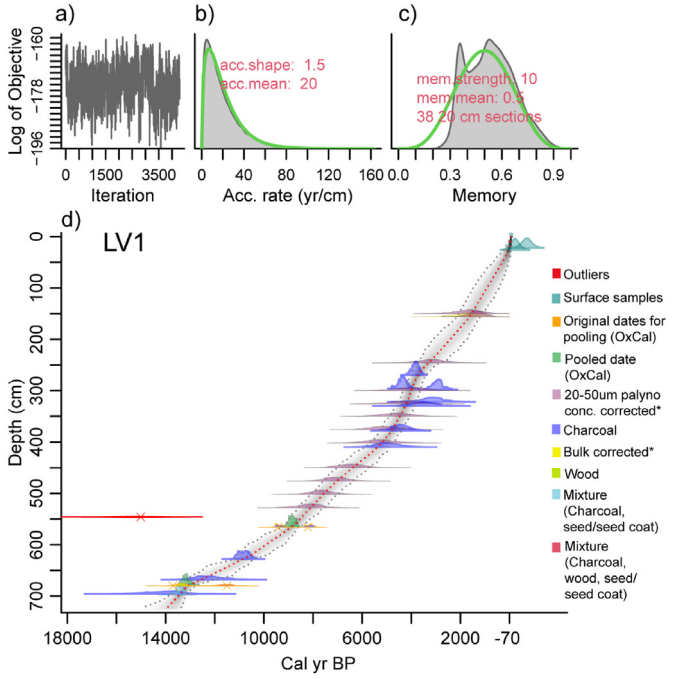

Fig. 2. Age-depth model of LV1, using the software Bacon (Blaauw and Christen, 2011; Blaauw et al., 2021) in cal yr BP (BP = 1950 CE; -70 = 2020 CE). (a) Markov Chain Monte Carlo random walk model iterations. (b) Prior (green) and posterior (grey) distribution of accumulation rate. (c) Prior (green) and posterior (grey) distribution of the age model. (d) Calibrated ^{14}C dates and age-depth model results. The red line indicates the best fit central tendency estimate for the model based on the weighted mean of all included iterations. The grey shade indicates a summary of the iterative walks, and the grey dotted line shows the 95% confidence intervals of these iterations. *20–50 μm palynomorph concentrate corrected for ^{14}C reservoir effect. (For interpretation of the references to colour in this figure legend, the reader is referred to the Web version of this article.)

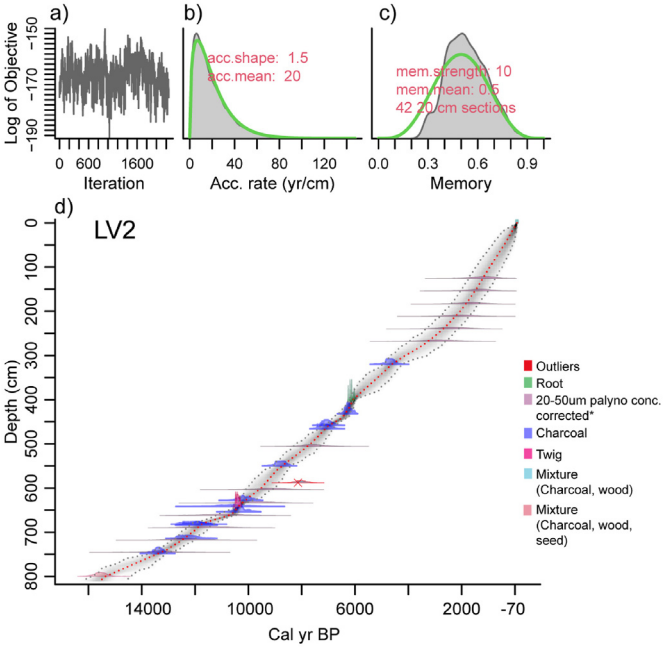

Fig. 3. Age-depth model of LV2 using Bacon software (Blaauw and Christen, 2011; Blaauw et al., 2021) in cal yr BP (BP = 1950 CE; -70 = 2020 CE). (a) Markov Chain Monte Carlo random walk model iterations. (b) Prior (green) and posterior (grey) distribution of accumulation rate. (c) Prior (green) and posterior (grey) distribution of the age model. (d) Calibrated ^{14}C dates and age-depth model results. The red line indicates the best fit central tendency estimate for the model based on the weighted mean of all included iterations. The grey shade indicates a summary of the iterative walks, and the grey dotted line shows the 95% confidence intervals of these iterations. *20–50 μm palynomorph concentrate corrected for ^{14}C reservoir effect. (For interpretation of the references to colour in this figure legend, the reader is referred to the Web version of this article.)

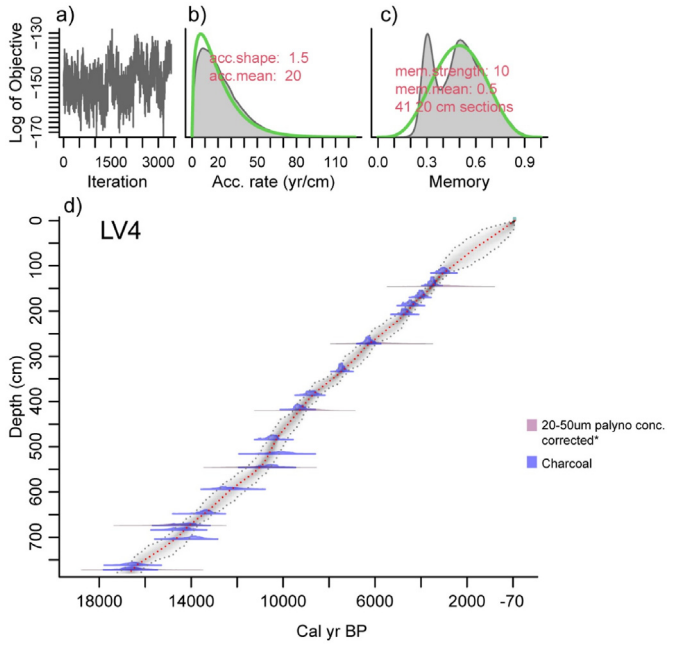

Fig. 4. Age-depth model of LV4, using the software Bacon (Blaauw and Christen, 2011; Blaauw et al., 2021) in cal yr BP (BP = 1950 CE; -70 = 2020 CE). (a) Markov Chain Monte Carlo random walk model iterations. (b) Prior (green) and posterior (grey) distribution of accumulation rate. (c) Prior (green) and posterior (grey) distribution of the age model. (d) Calibrated ^{14}C dates and age-depth model results. The red line indicates the best fit central tendency estimate for the model based on the weighted mean of all included iterations. The grey shade indicates a summary of the iterative walks, and the grey dotted line shows the 95% confidence intervals of these iterations. *20–50 μm palynomorph concentrate corrected for ^{14}C reservoir effect. Dates coming from the 20-50 μm palynomorph concentrate appear in the diagram with larger uncertainties behind the charcoal dates. (For interpretation of the references to colour in this figure legend, the reader is referred to the Web version of this article.)

latter may have increased by human impact in the catchment during the past 2000 years (Clark, 1962). LV4 does not show such a pattern, suggesting that in the deeper parts of the lake sedimentation rates remained more stable during the Late Glacial and the Holocene.

3.2. Macroscopic charcoal and fire history

CHAR values differ between sites (Fig. 5f) showing p values < 0.05 (Mann–Whitney test) when compared with each other. Charcoal influx ranges at LV1 from 0 to 2.12 particles cm^{-2} yr^{-1}, at LV2 from 0 to 0.89 and, at LV4 from 0 to 3.02, with means of 0.04, 0.08, and 0.15 particles cm^{-2} yr^{-1}, respectively. The variability of records through time follows similar trends. LV1 shows more homogeneous and lower values than the other two sites possibly as a consequence of the morphology of the coring location and sediment resuspension (Fig. 5f). These moderate differences between sites might indicate that there are also various physical factors acting on charcoal transport and/or charcoal sources, such as water circulation, and depositional environments. In these terms, it has been demonstrated that, throughout the year Lake Victoria has a significant movement of waters across all its extension (Nyamweya et al., 2016). Therefore, we primarily attribute the deposition of the biggest charcoal particles at LV4 to sediment focusing in the deepest part of lake (Blais and Kalff, 1995).

At LV4, which is the chronologically best dated and the longest sequence, trend lines show CHAR maxima lasting from ca. 15,000–14,000, 11,500–10,500 and 5000–4000 cal yr BP. The latter maximum also occurs at the two other sites and is thus reproducible in space and time, attesting to a definite increase in biomass burning around 5000–4000 cal yr BP (Fig. 5). Declining trends in CHAR fluxes occur at all three sites from 13,000 to 11,500 cal yr BP, suggesting weakening burning during this time. From 10,000–5000 cal yr BP, CHAR fluxes remain low at all three sites, suggesting that fire events were reduced in the Lake Victoria basin during this time. A period with declining CHAR trends occurred again at all three sites from 4000 to 2000 cal yr BP, suggesting that after the fire peak at around 4500 cal yr BP, regional burning decreased for approximately two millennia. Change points occurred during periods showing divergent patterns of CHAR, being minima (e.g. 16,660 cal yr BP), increases (e.g. 15,090 cal yr BP), maxima (e.g. 11,150 cal yr BP), and declines (e.g. 2660 cal yr BP). In sum, LV4 CHAR change points occur at ca. 16,660, 15,090, 11,150, and 2660 cal yr BP (Fig. 5 d,e).

3.3. Palynology and vegetation history

We identified three statistically significant local pollen assemblage zones (LPAZ), at all three sites (Figs. 6–8). A subzone boundary was added visually to LV2 and LV4, where the sequence is older. Pollen did not reach sufficient counts in the deepest sediments of LV4; specifically pollen grains and palynomorphs were absent at the bottom, and as we moved up core, a few corroded pollen grains and *Botryococcus* and *Pediastrum* occurred. After ca. 16,000 cal yr BP, the number of pollen grains was sufficient to reach statistically meaningful counts. The timing of the boundaries between sites differs slightly due to the variation in the chronologies between sites, but these differences are within the limits of the age uncertainties. For this reason, the chronology taken into account to define the LPAZ is that belonging to LV4.

LPAZ LV2-1a, LV4-1a (LV2: 806–760 cm; LV4:778–640 cm, ca. ***16,660–13,230 cal yr BP****)*: Poaceae is the most abundant taxon (>65%), followed by Cyperaceae and *Cyperus*-type (ca. 10%) and Amaranthaceae/Chenopodiaceae (ca. 3%), suggesting open vegetation conditions during this period, most likely savanna ecosystems also characterized by genera such as *Combretum*. Afromontane components, mostly *Olea* and *Podocarpus,* likely built substantial stands after ca. 13,500 cal yr BP in the Lake Victoria area. The conspicuous presence of *Typha* pollen (>5%) suggests local swampy conditions at the sites LV2 and LV4, probably as a result of low lake levels and thus dry environments. CHAR suggests that fire burning was very low at ca. 16,000–15,000 cal yr BP, and started to increase between 15,000 and 14,000 cal yr BP.

LPAZ LV1-1, LV2-1b, LV4-1b (LV1: 722–611 cm; LV2: 804–656 cm; LV4:640–529 cm, ca. ***13,230–10,750 cal yr BP****)*: Poaceae (<50%), Cyperaceae (ca. 10%), and *Cyperus*-type (ca. 10%) pollen values remain high and stable, suggesting the persistence of savanna ecosystems. Taxa such as *Alchornea*, *Urera*-type and a very few trees such as *Celtis* and *Podocarpus* likely established locally, while Afromontane *Olea* (>15%) populations expanded during this time. The pollen data suggest that *Typha* populations decreased at the coring sites, likely because the local swamps or ponds were inundated. Moreover, the pollen data (e.g. Moraceae, *Celtis*, *Podocarpus*, *Olea*) suggest that transitional and river rainforest stands established when burning declined.

LPAZ LV1-2, LV2-2, LV4-2 (LV1: 611–296 cm; LV2: 656–305 cm; LV4: 529–223 cm, ***ca. 10,750–5020 cal yr BP****)*: Poaceae pollen rapidly declines (<20%), as do Cyperaceae and *Cyperus*-type (<5%), while pollen of Moraceae, *Acalypha*, *Alchornea,* and *Urera*-type increases massively, suggesting that savanna ecosystems were replaced by rainforests during the early Holocene. Furthermore, the pollen data suggest that Afromontane forests also spread at the expense of grasslands and savanna during this period, although less pronounced than the rainforests. *Celtis* populations expanded,

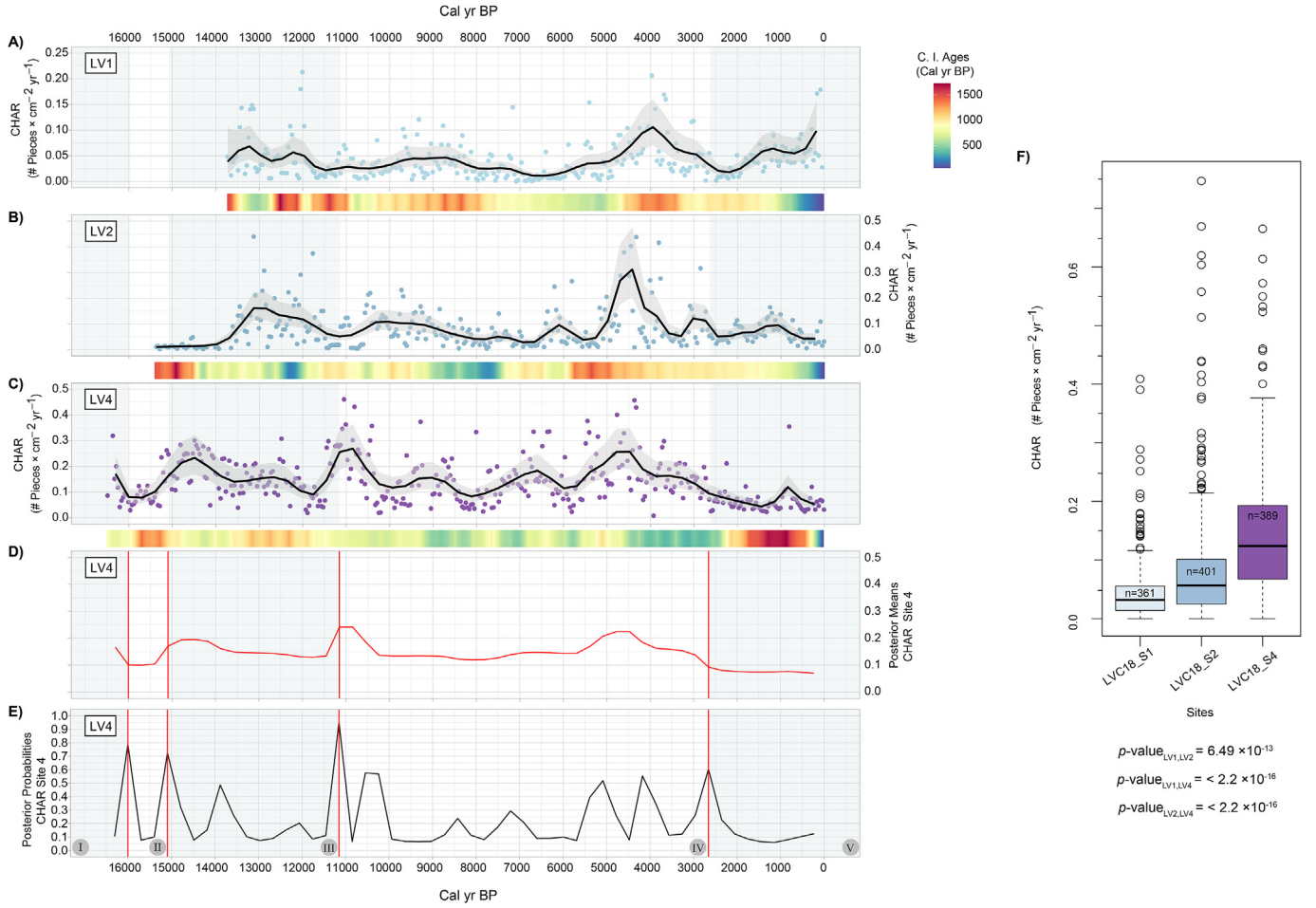

Fig. 5. (a) Macrocharcoal record from LV1, (b) macrocharcoal record from LV2, (c) macrocharcoal record from LV4. For (a), (b), and (c), coloured points represent each sample, the black continuous line indicates a trend line based on a GAM, the grey shaded envelope represents the 95% confidence interval for the plotted trends, the grey shaded areas mark the time span between each change point, and coloured bars under each site represent the confidence interval (C.I.) age range for each point according to each age-depth model. (d) Posterior means for CHAR record from LV4 after Bayesian change point analysis. (e) Posterior probabilities of a change point for each position in the sequence of observations from ca. 16,600 cal yr BP to the present: red lines mark the exact position of each change point, and numbers in the grey circle indicate the number of each change point for reference in the text. (f) Boxplot showing the distribution of charcoal influx (CHAR) at the three sites. (For interpretation of the references to colour in this figure legend, the reader is referred to the Web version of this article.)

peaking at ca. 8000–6000 cal yr BP during the mid-Holocene (ca. 25%), while *Olea* gradually declined. The massive rainforest expansion was accompanied by steadily declining fire activity from 10,000–5000 cal yr BP, suggesting that rainforest reduced regional burning. The fire minimum of the whole record was reached between ca. 9000 and 7000 cal yr BP, when Moraceae and thus the rain forests peaked.

LPAZ LV1-3, LV2-3, LV4-3 (LV1: 296–0 cm; LV2: 305–0 cm; LV4: 223–0 cm, ***ca. 5020 cal yr BP–Present****):* Pollen of rainforest taxa (e.g. Moraceae, Urera-type, *Alchornea*) declines and Poaceae and other savanna taxa (e.g. *Combretum*) increase from 25% to 50%, marking the onset of the late Holocene savanna re-expansion. The pollen data suggest that the Afromontane vegetation also declined, though less pronouncedly than the rainforest. Interestingly, close to the onset of this LPAZ at ca. 4800 cal yr BP, fire disturbance peaked, and *Podocarpus-Juniperus* forests expanded. The gradual decline of burning after a maximum at ca. 4500 to 3000 cal yr BP seems to be linked to the expansion of savanna ecosystems; it might thus be related to decreasing fuel availability during the late Holocene. However, fire incidence slightly increased after 1000 cal yr BP in connection with a further expansion of savanna, suggesting that the linkage between fuel availability and biomass burning does not always follow the same pattern.

3.4. Ordination analyses

When performing the analysis site by site, we obtained similar patterns to the ones shown in the PCA, which includes all sites. Therefore, we decided to show the one for LV4 (Fig. 10) because it includes a larger time span and a summary PCA including all sites (Fig. 11). For the PCA of LV4 (Fig. 10), the first two axes explain 85.48% of the total variance in the pollen data, of which 73.45% is explained by PC axis 1 and 12.03% by PC axis 2. For the summary PCA (Fig. 11), the first two axes explain 74.72% of the total variance, of which 59.33% is explained by PC axis 1 and 15.39% by PC axis 2.

For both PCAs, axis 1 spans a gradient from positive species scores such as Cyperaceae, *Juniperus*, *Typha angustifolia,* and *Cyperus*-type to negative species scores such as Moraceae, *Celtis*, and *Alchornea*. Thus, axis 1 may reflect an environmental gradient from warmer and wetter conditions (Moraceae, *Alchornea*, *Celtis*) to drier conditions (Amaranthaceae/Chenopodiaceae, Poaceae), with water plants such as *Typha* mirroring low lake levels. This interpretation

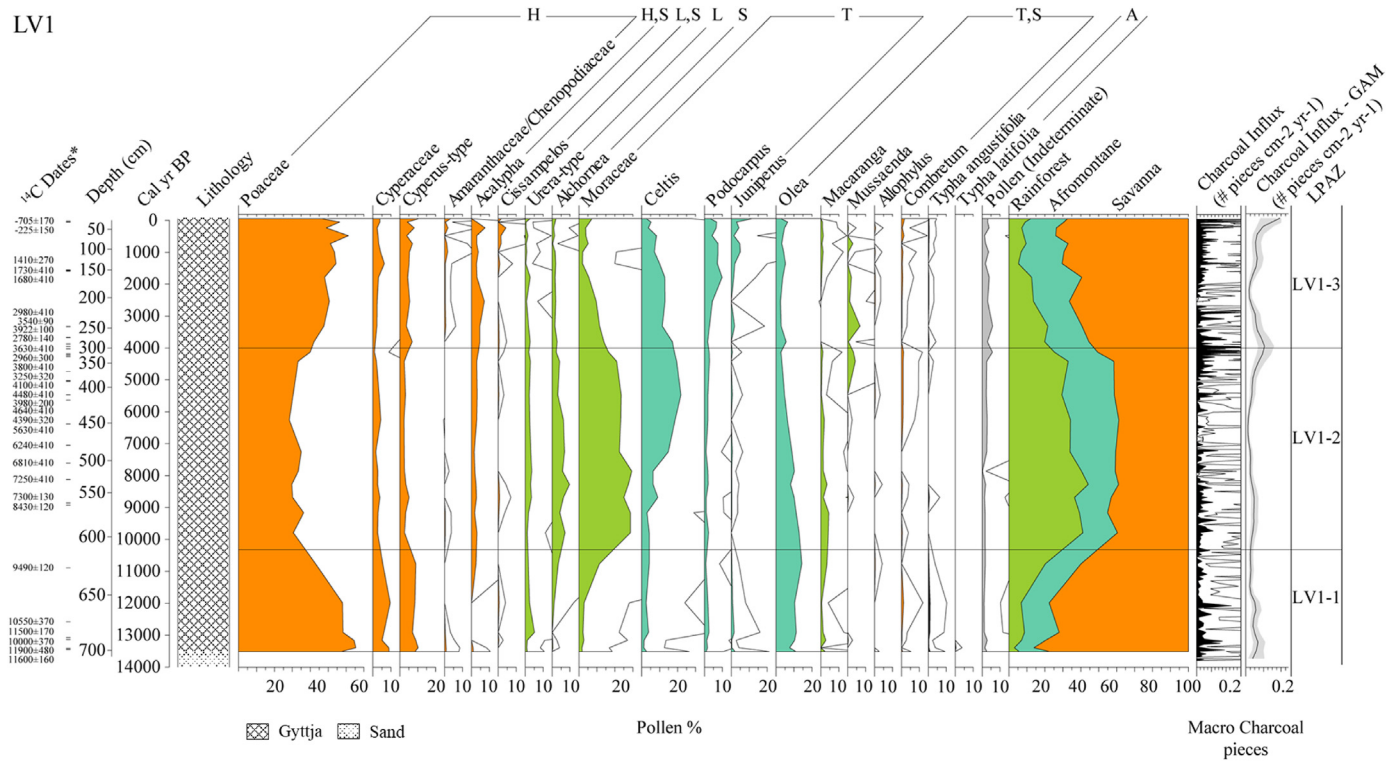

Fig. 6. Pollen percentages and macroscopic charcoal concentration values of the LV1 record. LPAZ = Local pollen assemblage zones, H = herbs, S = shrubs, L = lianas, T = trees, A = aquatic. Empty curves represent a 10 × exaggeration. In the charcoal influx GAM trend, the grey shaded envelope represents the 95% confidence interval. *Dates rounded following Stuiver and Polach (1977).

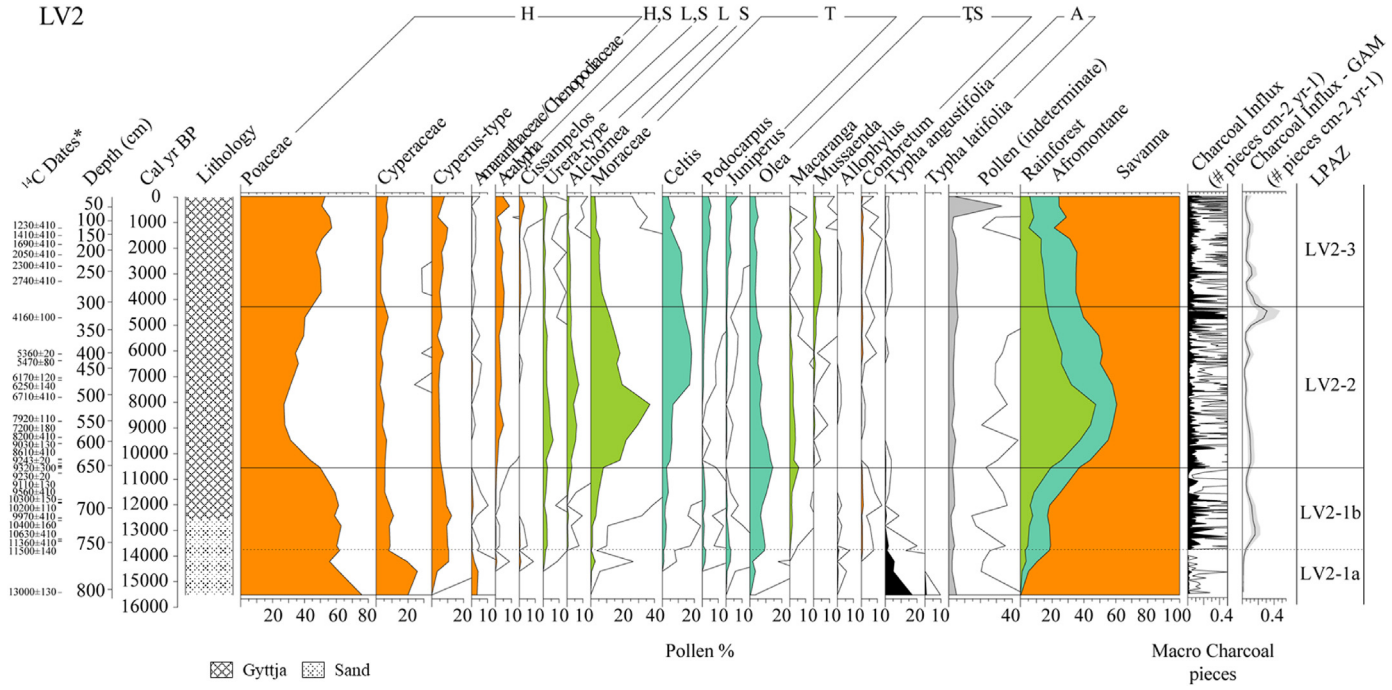

Fig. 7. Pollen percentages, and macroscopic charcoal concentration values of the LV2 record. LPAZ = Local pollen assemblage zones, H = herbs, S = shrubs, L = lianas, T = trees, A = aquatic. Empty curves represent a 10 × exaggeration. In the charcoal influx GAM trend, the grey shaded envelope represents the 95% confidence interval. *Dates rounded following Stuiver and Polach (1977).

is corroborated by the passively added TEX 86 data in °C for Lakes Tanganyika, Victoria, and Chala (Figs. 10–11). On axis 2, the most positive species scores belong to *Celtis*, *Mussaenda*, *Podocarpus*, and *Juniperus*, and the most negative are reached by *Macaranga*, *Olea*, and *Urera*. Therefore, we infer that axis 2 is connected to a gradient from denser (*Mussaenda*, *Podocarpus-Juniperus*) forest to more

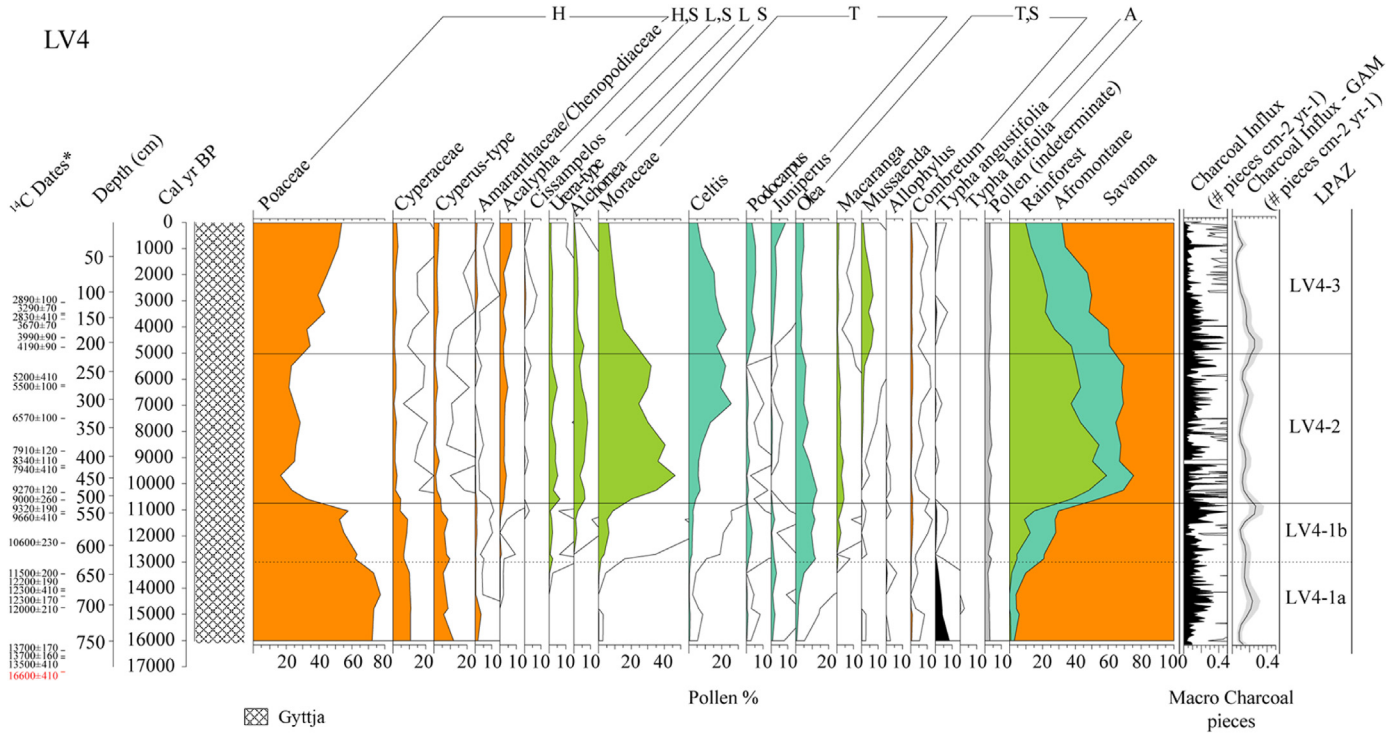

Fig. 8. Pollen percentages, and macroscopic charcoal concentration values of the LV4 record. LPAZ = Local pollen assemblage zones, H = herbs, S = shrubs, L = lianas, T = trees, A = aquatic. Empty curves represent a 10 × exaggeration. In the charcoal influx GAM trend, the grey shaded envelope represents the 95% confidence interval. The radiocarbon date marked in red represents the dated sediment recovered from the core catcher below the last segment core (below 778 cm). *Dates rounded following Stuiver and Polach (1977). (For interpretation of the references to colour in this figure legend, the reader is referred to the Web version of this article.)

open (*Olea*) and pioneer communities (*Macaranga*), probably reflecting the importance of light availability. Interestingly, charcoal as a fire proxy is only weakly associated with axis 2, suggesting that at multimillennial scales vegetation and fire were linked at a secondary order of importance when compared to the linkage between vegetation and temperature.

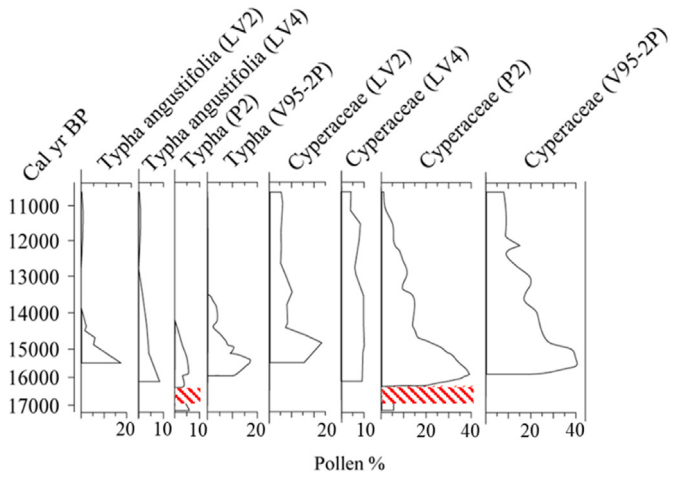

Fig. 9. Pollen percentages of *Typha* and Cyperaceae from 11,000 to 17,000 cal yr BP of LV2 and LV4 (this study) compared with same pollen species from P2 (Kendall, 1969) and V95–2P (Beuning, 1999). Red lines represent the time gap of a sediment discontinuity reported by Kendall (1969). (For interpretation of the references to colour in this figure legend, the reader is referred to the Web version of this article.)

4. Discussion

4.1. Chronological framework

Due to the size of Lake Victoria, it is difficult for big macrofossils to deposit there, thus it is challenging to find optimal material for radiocarbon dating. Various studies have used two distinct types of material for radiocarbon dating: 1) bulk lake sediment including filtered concentrates of 20–70 μm supposed to contain a mix of pollen, lignin, and charcoal (Kendall, 1969; Stager, 1984; Stager et al., 1986, 1997) and 2) charcoal (Beuning, 1999; Beuning et al., 1997; Johnson et al., 1996). Even though the resulting chronological models provide the closest accuracy to the real ages of the lake deposits, several sources of contamination are known to affect the age determination of bulk and other nonterrestrial organic material (Walker, 2005). These include factors such as the reservoir effect, the mineral carbon error, and the presence of residues from aquatic organisms, which may have taken up old carbon from the water and sediments.

Several correction factors have been applied to account for the reservoir effect, all of them constant over time. In all studies, the reservoir effect was considered constant through time. Kendall (1969) proposed a 'zero error' of 400 years by extrapolation of the mean wet sediment rate of the surface muds from Lake Victoria's Pilkington Bay. However, Stager et al. (1997) reported a 600 year reservoir effect based on a linear extrapolation from the ages of a top core from Damba Channel, estimations for the P2 core (Stuiver, 1970). Later, Beuning et al. (1997) and Johnson et al. (1998) suggested a 500 year reservoir effect.

Our estimations of a 573 year ^{14}C reservoir effect, which are based on multiple date comparisons across three cores, refines

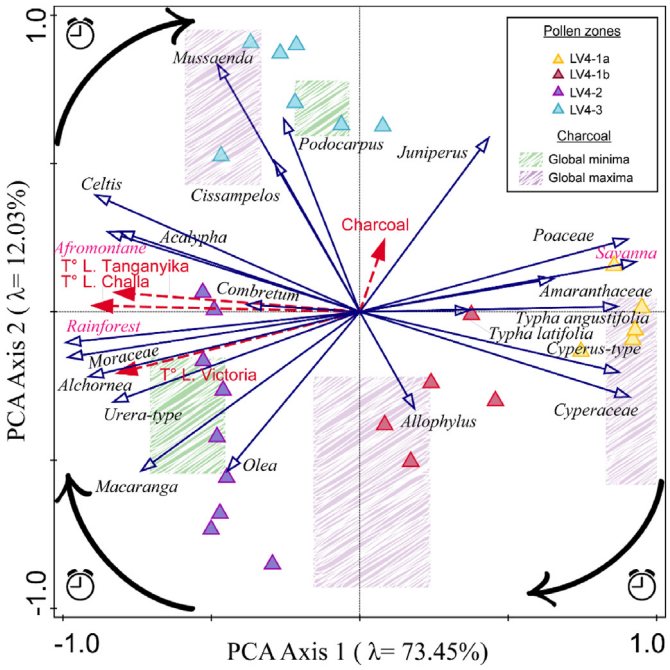

Fig. 10. Principal component analysis (PCA) triplot of LV4 showing response variables (pollen taxa and biome sums, blue arrows), passive variables (temperature and charcoal, red arrows), and sample scores which are indicated with symbols. Different colours represent the local pollen zones and subzones. PCA axis 1 explains 73.45% of the variance, and PCA axis 2 explains 12.03% of the variance. Coloured rectangles represent localization of global maxima and minima in charcoal influxes in accordance with time (this study). Arrows represent the direction of time in the record according to the sample scores. Temperature records were obtained from TEX_{86} data for Lake Tanganyika (Tierney et al., 2008), Lake Victoria (Berke et al., 2012), and Lake Chala (Sinninghe Damsté et al., 2012). (For interpretation of the references to colour in this figure legend, the reader is referred to the Web version of this article.)

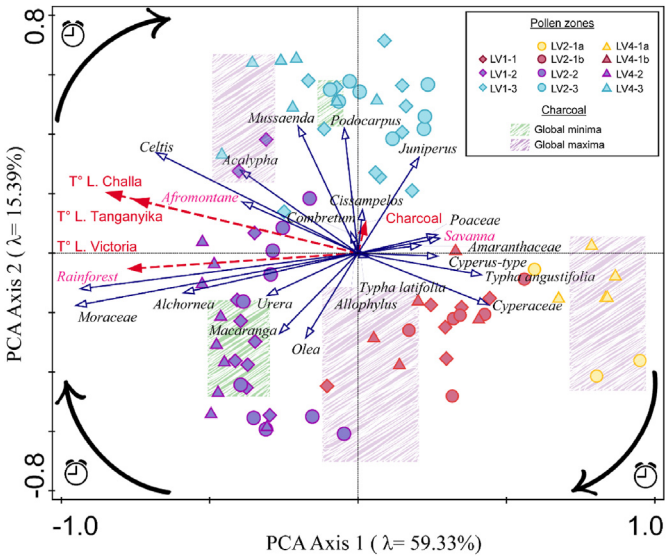

Fig. 11. Principal component analysis (PCA) triplot of all sites showing response variables (pollen taxa and biome sums, blue arrows), passive variables (temperature and charcoal, red arrows), and sample scores which are indicated with symbols. Different symbols represent the sites, and colours represent the local pollen zones and subzones. PCA axis 1 explains 59.33% of the variance, and PCA axis 2 explains 15.39% of the variance. Coloured rectangles represent localization of global maxima and minima in charcoal influxes in accordance with time (this study). Arrows represent the direction of time in the record according to the sample scores. Temperature records were obtained from TEX_{86} data for Lake Tanganyika (Tierney et al., 2008), Lake Victoria (Berke et al., 2012), and Lake Chala (Sinninghe Damsté et al., 2012). (For interpretation of the references to colour in this figure legend, the reader is referred to the Web version of this article.)

earlier estimates. The difference of 570 years falls between the corrections of 400 years for the P2 core (Kendall, 1969), 500 years for V95–2P (Beuning et al., 1997), and 600 years for Ibis 2 (Stager et al., 1997). Kendall (1969) also mentions that the radiocarbon dates in his study were calculated with a ^{14}C half-life of 5568 years instead of 5730 as today, changing the value of the dates by a factor of 1.03. Such a good agreement implies that the previous chronological estimations were done carefully and are comparable with ours, having a correction of 500–600 years, or slightly less (400 years), given that the dating uncertainties often span several centuries (Table 1). For instance, the uncertainties of the reservoir effect were identified as 51–82 years (Beuning et al., 1997); 50–140 years (Johnson et al., 1998), 60–200 years (Kendall, 1969), and 80–300 years (Stager et al., 1997). However, the age gaps between the material dated are large, increasing the uncertainties of these models. Hence, this paper relies on many more charcoal dates than any other study to build the age–depth models, so that we can reduce the temporal uncertainties of the different events recorded in the lake sediments.

Kendall (1969) reported a stratigraphic discontinuity, which lasted until ca. 16,500 cal yr BP. However, this discontinuity layer was not present in the sediment of LV4. We know that in terms of time we are situated at the top of this layer because of the biostratigraphic relations that we can observe not only in this study but also in Beuning's (1999). These include the high values of *Typha, Olea* and Cyperaceae.

In contrast to the continuous gyttja layer that we see throughout the LV4 core, reaching the oldest dates of 16,100–17,000 cal yr BP for the core (19,000-21,000 cal yr BP for the sediment below it) (Table 1), Beuning (1999) found a 'vertisol' with rootlets and reed stems. That layer extended from 16,100 to ca. 15,500 cal yr BP with a peak in Cyperaceae and *Typha* that was found in our study in core LV4 (Fig. 9) and in core P2 (Kendall, 1969). Interestingly, a sandy layer also occurs in the shallower cores LV1 and LV2 presented here (Figs. 1, 6-9). This difference between LV4 and the other cores most likely indicates shallow water or swampy conditions at the profundal site, while probably shore conditions occurred at the shallower sites. Moreover, local shallower conditions inferred close to the other sites of coring, P2, V95–2P, LV1 and LV2, would then imply that the north and eastern parts of Lake Victoria were affected by very low water levels, whereas LV4 (deepest coring site) would have maintained relatively higher water tables around 16,100–17,000 cal yr BP. However, prior to 16,000 cal yr BP, lake levels must have been quite low also at LV4 (Fig. 9), as indicated by the high abundances of the swamp or lakeshore plant *Typha* (>5%). Higher water tables at LV4 than at the other sites around 16,000 cal yr BP may explain the relatively low abundances of Cyperaceae, which was likely growing in marshy or swampy reeds close to the shore (<10 vs. 35–40%, Fig. 9).

The timing of the population peak of *Typha* at ca. 16,500–14,500 cal yr BP in the Lake Victoria records (Beuning, 1999; Kendall, 1969; this study, Fig. 9) coincides with that observed from 16,500 to 14,000 cal yr BP at Lake Rukwa (Vincens et al., 2005). Taken together, the available evidence suggests that a regional eastern African lake desiccation phase may have started before 18,500 cal yr BP and lasted until ca. 16,000–15,500 cal yr BP (*Typha* and Cyperaceae peaks in this study, Vincens et al., 2005). This dry phase was then followed by a wetter period that lasted until about 13,000 cal yr BP, when *Typha* and Cyperaceae began to decline.

4.2. Biome interactions with climate and fires

The role that temperature, moisture, slopes, wind, and fuel play in the occurrence of fire events and the importance of human activities and vegetation as drivers of fire regimes have been extensively discussed (e.g. Archibald et al., 2009; Marlon, 2020). Whereas fire activity is co-modulated by fire-weather conditions involving heat, moisture, and wind, and vegetation composition and structure determines fuel availability, humans today are an important source of fire ignition (Conedera et al., 2009). Across the planet, the distribution of climatic mechanisms is broad, and throughout the late Pleistocene and the Holocene especially in the tropical regions, some climatically important events have occurred. In eastern Africa, past fire occurrence is likely to have been primarily driven by two factors: climatic conditions, which determine temperature, rainfall, the length of the dry and wet seasons and thus moisture availability (Nelson et al., 2012); and biomass availability, which depends on the climatically controlled biome type (e.g. Schüler et al., 2012) and within the Afromontane regions, the vegetation type (Hemp, 2005; Hemp and Beck, 2001; Mustaphi et al., 2021). However, even within the same kind of ecosystem, slight changes in moisture balance cause variations in fire propensity as observed previously in equatorial eastern Africa (Colombaroli et al., 2014; Gillson, 2004).

Major climatic changes altered past sea surface temperatures (SST) and with it, patterns in rainfall; for instance, during Heinrich Event 1, a megadrought occurred in the Afro–Asian Monsoon region, which Stager et al. (2011) attributed to a movement of the Intertropical Convergence Zone (ITCZ) between 17,000 and 16,000 cal yr BP. This episode caused effects across eastern Africa, such as diatom-inferred low-water stands in Lake Tanganyika (Stager et al., 2011), the drying out of Lake Tana (Lamb et al., 2007), and swampy conditions in Lake Rukwa (Vincens et al., 2005). Moreover, climate may have influenced the fire regime through vegetation, for instance by promoting the growth of flammable dry savanna around Lake Victoria at ca. 15,000 to 14,000 cal yr BP. The flammable savanna persisted until the onset of the Holocene, although more mesophilous Afromontane taxa such as *Olea* and *Podocarpus* expanded between 16,000 and 12,000 cal yr BP. It is unclear whether this conspicuous Late Glacial expansion of subtropical Afromontane vegetation (Figs. 6–8; Kendall, 1969) was the consequence of colder-than-today conditions in the Lake Victoria area, or less likely, whether it was caused by increased wind transport of pollen from higher altitudes (Kendall, 1969; Beuning, 1999). Indeed, today Lake Victoria is only ca. 100–200 m below the lowest Afromontane forest stands, which implies that cooling of 1–2 °C would be enough to promote the expansion of subtropical vegetation close to the lake shores, if moisture is sufficient regionally, or locally along riverine fringes (Schüler and Hemp, 2016). Moreover, this cooling would partly push the rainforest vegetation below the site as subtropical Afromontane vegetation expanded. This cooler situation, besides the reduced moisture availability, may also explain the strong reduction in rain forest vegetation during the Late Glacial around Lake Victoria. Indeed, between 16,000 and 12,000 cal yr BP, annual mean temperatures oscillated between 19 and 23 °C in the Lake Victoria area (Berke et al., 2012), thus creating a suitable environment for Afromontane vegetation (see introduction). Further evidence for the temperature sensitivity of rainforests comes from our ordination analyses (Figs. 10 and 11), which suggest that temperature primarily influenced tropical vegetation and that its influence on the fire regime was of secondary importance and/or mediated through vegetation.

From 12,000–9000 cal yr BP, biomass burning increased over Africa (Power et al., 2008). At the onset of the Holocene, atmospheric circulation was enhanced, which in eastern Africa resulted in a long-term increase in African monsoon activity and marked latitudinal shifts of the ITCZ (Garcin et al., 2007). In the equatorial tropics, this shift brought a pronounced increase in precipitation and a decrease in wind speed (Talbot et al., 2007). At Lake Victoria, this climatic shift resulted in a significant drop in fire occurrence, which persisted for several millennia through the early and mid-Holocene (Fig. 9). The decline of burning, which reached its lowest point at around 8000–6000 cal yr BP, was likely caused by warm and moist conditions, which also promoted the large-scale expansion of rainforests in the Lake Victoria area. We assume that during that time the fire regime shifted from fuel limited, due to the low biomass of dry savanna, to moisture limited due to the high biomass of humid rainforest. Most likely, the fire regime shift was accelerated by the reduced flammability of rainforest vegetation and positive feedbacks on moisture availability associated with the expansion of dense forest canopy (Ivory and Russell, 2016). During the Holocene, the African Humid Period promoted the expansion of tall and partly shade-tolerant tropical rainforest trees and lianas such as Moraceae, *Macaranga, Alchornea*, *Acalypha*, and *Urera* at the expense of herbaceous savanna plants such as Poaceae and Amaranthaceae/Chenopodiaceae and shrubby trees such as *Combretum*. Afromontane trees such as *Olea* and *Podocarpus* likely moved several hundreds of meters upslope as a result of early and mid-Holocene climate warming. Increased moisture availability probably caused a general spread of *Celtis* to the lowlands around Lake Victoria, partly replacing the savanna during the mid-Holocene, a phase of low fire occurrence (Figs. 6–8; Schüler and Hemp, 2016).

Towards the end of the mid-Holocene at 6000–5000 cal yr BP, the monsoonal circulation changed, likely as a result of a weakening of summer insolation in North and eastern Africa (Demenocal et al., 2000; Vincens et al., 2005; Wirrmann et al., 2001). Convective precipitation declined, resulting in drier climates in the surroundings of Lake Victoria and releasing the retreat of rainforests and the re-expansion of savanna vegetation. It is likely that this climatic shift to drier conditions (e.g. Schüler et al., 2012) and the resulting vegetation change caused the biomass-burning maximum at ca. 5000 cal yr BP. By the midst of the late Holocene, as rainy conditions re-emerged across tropical Africa (Gasse, 2000), moisture reduced the development of fires, giving rise to the last minimum in the record between ca. 3000 and 2000 cal yr BP under a vegetation mix of savanna, rainforest, and Afromontane vegetation. Concurrently, metal-using agriculturalists spread in Eastern Africa (Clark, 1962; Kendall, 1969), likely contributing to major vegetation changes (Huffman, 1982; Humphris and Iles, 2013; Iles and Lane, 2015; M'Mbogori, 2021) and gradually resulting in the greatest landscape alterations by around 1500 cal yr BP (Schoenbrun, 1998). However, although this archaeological evidence is broadly accepted (e.g. Desmedt, 1991; Goldstein and Munyiri, 2017; Huffman, 1982; Marchant, 2021; Schoenbrun, 1993), palynological indicators for such a change have remained elusive (Beuning, 1999; Marchant et al., 2018). In our study, we focused on fire regime changes, and the vegetation overview used for biome reconstruction is too coarse to disentangle human modifications to ecosystems. Further high-resolution analyses are needed to better assess the human influence on the fire regime and vegetation.

5. Conclusion

This study provides a reliable chronological framework from an intensively dated transect across Lake Victoria. We conclude that climate was the main driver of fire in this area, at least until the early Iron Age (ca. 2400–1100 yr BP), when human impact became important. The regional fire regime and vegetation changes seem to

function concomitantly. Fire occurrence may have been controlled by combined factors, such as fuel availability, heat, and moisture occurrence. Under dry and warm climates, when savanna expanded, fire occurrences increased; conversely, warm and humid climates promoted rain forests and reduced fire ignition and spread. The Lake Victoria basin, where tropical rainforest, savanna, and subtropical Afromontane vegetation co-occur, has been shown to be very sensitive to subtle climatic changes; even 1–2 °C may drive biome reorganizations. Thus, even minor future increases in temperature may provoke major ecosystem shifts, which may in turn affect the fire regime. Therefore, conservation measures are needed to prevent drastic impacts and reduce ecosystem vulnerability under global change conditions. Two plausible actions are to enhance the existing sinks (forests) in order to store greenhouse gasses and to develop appropriate land use strategies to allow society and wildlife to adjust to ongoing and future climate change.

Author contributions

Author contributions of the article are as follows: YT, WT and EG conceptualized the study. BV assessed the fire reconstructions. JvL and YT conducted the palynological investigations. YT did the numerical investigations, the data visualisation and wrote the draft of the manuscript. EG, BV, JvL, GW, SS, CCM, MK, MM, OS, MG and WT discussed the results and commented on the manuscript. OS and MG acquired the funding. All authors agree on the science and the style of the manuscript.

Declaration of competing interest

The authors declare that they have no known competing financial interests or personal relationships that could have appeared to influence the work reported in this paper.

Data availability

The datasets will be available from Neotoma and the Alpine Palynological Data-Base (ALPADABA).

Acknowledgments

The authors Yunuén Temoltzin–Loranca, Giulia Wienhues, and Moritz Muschick were supported by SNSF Sinergia grant number 183566 awarded to Ole Seehausen, Martin Grosjean, Tom Gilbert, and Blake Matthews. The coring in Lake Victoria was financed by the strategic pool of the Faculty of Natural Sciences of University of Bern (grant to Ole Seehausen, Anna Sapfo Malaspinas, Willy Tinner, Oliver Heiri, Martin Grosjean, and Flavio Anselmetti) and the Institute of Plant Sciences of University of Bern. We gratefully acknowledge the coring leaders Petra Boltshauser-Kaltenrieder, Moritz Muschick, Salome Mwaiko, and Willi Tanner and the coring team members Sandra Brügger and Alexander Bolland. We thank Edith Vogel and Gary Salazar for their contribution to the ^{14}C analysis. We acknowledge the lab assistance of Lara Zinkl and Sara Brechbühl. We are deeply indebted to TAFIRI and its coring members for looking after the team and the coring platform during the expedition: Edwin Sombe (boat captain), Harith Kalima (engineer), Boaz Jumbe (crew), Toto Mohammed (technician), Daniel Bwathondi † (crew), Daniel Chacha (crew), and Hamisi Ramadhani (cook). We thank TAFIRI for all the logistic support during the campaign. This research was supported by TAFIRI and conducted under COSTECH research permit No. 2018-237-NA-2018-57. We are grateful to Lisa Schüler for offering an introduction to East African pollen grains and for making available the pollen reference collection of the Mount Kilimanjaro area. Hermann Behling is gratefully acknowledged for hosting Yunuén Temoltzin-Loranca at the Department of Palynology and Climate Dynamics at the University of Göttingen. We thank Gianni Zanchetta and Richard Vachula for their careful reading of our manuscript and their insightful comments and suggestions.

Appendix A

Methodology followed for sieving

When starting to sieve, it is important to subsample first and to avoid letting the samples to sit for more than 3 days in the fridge because they dry out, which makes them more difficult to sieve. The sequence of subsampling and sieving is always done from the bottom to the top of the core.

Subsampling

1. Clean all the surfaces before start working and do not take more than 1 core at a time.
2. Take out from the fridge only the section core needed.
3. Follow the composite file, which indicates the slices of 2 cm to be taken together.
4. Make sure the containers for storing the samples are clean.
   a. Subsampling every centimetre (continuously) for pollen
   i. Label the container.
   ii. Weight the empty container and tare the balance.
   iii. Clean the surfaces of the sediment with a spatula.
   iv. Take 1 cm^3 from the core with the volumetric subsampler (make sure you do not touch the edges).
   v. Weight the sample and record it.
   vi. Put the lid on, and store it in zipper storage bags according to depth.
   vii. Put the samples in the freezer.
   b. Subsampling for sieving
   i. Clean the surface of the core by removing the first millimetre of the sediment using a spatula.
   ii. Mark slices of 2 cm according to the composite document
   iii. Take the corresponding container (already labelled) and rinse it with tap water.
   iv. Cut the slice, taking care to not touch the edges of the pvc tube (leave at least 2–3 mm of the edges of the sediment that are in direct contact with the tube).
   v. Weight the container and tare.
   vi. Put the sediment into the container and record its weight.
   vii. Fill it up with water.
   viii. Put these samples in the fridge.

Sieving for macrofossils and charcoal

Due to the sensitivity of fish macrofossils used for other studies, the use of chemicals for extracting charcoal particles is not feasible. Therefore, conventional methods for deflocculating the sediment (Millspaugh and Whitlock, 1995; Mooney and Tinner, 2011) cannot be used. And sieving was done only with water.

For all depths, the sieving should be done with a tower of the 200μm and the 100μm sieve, with exception of samples located every 24 cm, where two extra sieves need to be added to the tower, 50μm and 20μm respectively.

To begin with the procedure, moisten all sieves (on both sides) with tap water, and proceed as follows:

1. Set up the sieving tower (accordingly)
   a. 200 and 100μm

or.

b. 200, 100, 50, and 20 μm
1. Put the sediment in the sieve
2. Place the sieving tower into a wet sieving machine and cover the uppermost sieve with the lid (make sure it is properly closed and the water hose is properly attached).
3. Adjust settings for a smooth oscillatory movement:
   a. Interval time: 6 s
b. Sieving time: 6 min
c. Amplitude: 0.8 mm

*The use of the sieving machine is solely to soften the sediment a little while soaking in water.

4. Turn on the tap (IN 2 INTERVALS), the first and second time only during 10 s with a low to medium water flow and a stop flow interval of ~3min. Before activating the movement of the machine, make sure that the uppermost sieve has always water on it (this step is important, because it avoids any possible breakage of particles).
5. Turn on the sieving machine.
6. Once the time is due, you can finish the sieving by hand (fine sieving).
7. Recover the remaining material in containers properly labelled using tap water.
8. Rinse the lid of the sieving machine every time the sample is changed.
9. Put the samples in the freezer.

Note:

In order to make sure that the macrofossils were not damaged in the sieving machine, a test was carried out in a total of 162 samples. Two samples were analysed in each depth. One being sieved completely manually and the other one with the aid of the machine at the beginning of the sieving procedure. Then, samples were compared to check for particles or macrofossil's breakage or damage.

There was no damage observed in chironomids, insect remains, fish scales, charcoal or fish teeth.

References

Adolf, C., Wunderle, S., Colombaroli, D., Weber, H., Gobet, E., Heiri, O., van Leeuwen, J., Bigler, C., Connor, S.E., Gałka, M., La Mantia, T., Makhortykh, S., Svitavská-Svobodová, H., Vanniere, B., Tinner, W., 2018. The sedimentary and remote-sensing reflection of biomass burning in Europe. Global Ecol. Biogeogr. 27 (2), 199–212.

Andama, M., 2012. Holocene climate and environmental history of Lake Victoria basin: evidence from geochemical proxies. Quat. Int. 279, 18.

Archibald, S., Roy, D.P., van Wilgen, B.W., Scholes, R.J., 2009. What limits fire? An examination of drivers of burnt area in Southern Africa. Global Change Biol. 15 (3), 613–630. https://doi.org/10.1111/j.1365-2486.2008.01754.x.

Behling, H., 2002. South and southeast Brazilian grasslands during Late Quaternary times: a synthesis. Palaeogeogr. Palaeoclimatol. Palaeoecol. 177 (1–2), 19–27. https://doi.org/10.1016/S0031-0182(01)00349-2.

Bennett, K.D., 1996. Determination of the number of zones in a biostratigraphical sequence. New Phytol. 132 (1), 155–170.

Berke, M.A., Johnson, T.C., Werne, J.P., Grice, K., Schouten, S., Damsté, J.S.S., 2012. Molecular records of climate variability and vegetation response since the late Pleistocene in the Lake Victoria basin, East Africa. Quat. Sci. Rev. 55, 59–74.

Beuning, K.R.M., 1999. A re-evaluation of the late glacial and early Holocene vegetation history of the Lake Victoria region, East Africa. In: van Zinderen Bakker, E.M., Heine, K. (Eds.), Palaeoecology of Africa and the Surrounding Islands. Routledge, pp. 115–136. First.

Beuning, K.R., Kelts, K., Russell, J., Wolfe, B.B., 2002. Reassessment of Lake Victoria–Upper Nile River paleohydrology from oxygen isotope records of lake-sediment cellulose. Geology 30 (6), 559–562.

Beuning, K.R.M., Kelts, K., Ito, E., Johnson, T.C., 1997. Paleohydrology of Lake Victoria, East Africa, inferred from18O/16O ratios in sediment cellulose. Geology 25 (12), 1083–1086.

Beverly, E.J., White, J.D., Peppe, D.J., Faith, J.T., Blegen, N., Tryon, C.A., 2020. Rapid Pleistocene desiccation and the future of Africa's Lake Victoria. Earth Planet Sci. Lett. 530, 115883. https://doi.org/10.1016/J.EPSL.2019.115883.

Birks, H.J.B., Gordon, A.D., 1985. Numerical Methods in Quaternary Pollen Analysis. Academic Press.

Blaauw, M., Christen, J.A., Aquino Lopez, M.A., 2021. Age-depth Modelling Using Bayesian Statistics, Package 'rbacon'.

Blaauw, M., Christen, J.A., 2011. Flexible palaeoclimate age-depth models using an autoregressive gamma process. Bayesian Anal. 6, 457–474.

Blais, J.M., Kalff, J., 1995. The influence of lake morphometry on sediment focusing. Limnol. Oceanogr. 40 (3), 582–588.

Bronk Ramsey, C., 1994. Analysis of chronological information and radiocarbon calibration: the program OxCal. Archaeol. Comput. Newsl. 41, 11–16.

Bronk Ramsey, C., 1995. Radiocarbon calibration and analysis of stratigraphy: the OxCal program. Radiocarbon 37 (2), 425–430.

Bronk Ramsey, C., 2001. Development of the radiocarbon calibration program OxCal. Radiocarbon 43 (2A), 355–363.

Burbridge, R.E., Mayle, F.E., Killeen, T.J., 2004. Fifty-thousand-year vegetation and climate history of noel kempff mercado national park, Bolivian Amazon. Quat. Res. 61 (2), 215–230. https://doi.org/10.1016/j.yqres.2003.12.004.

Clark, J.D., 1962. The spread of food production in sub-Saharan Africa. J. Afr. Hist. 3 (2), 211–228.

Colombaroli, D., Ssemmanda, I., Gelorini, V., Verschuren, D., 2014. Contrasting long-term records of biomass burning in wet and dry savannas of equatorial East Africa. Global Change Biol. 20 (9), 2903–2914. https://doi.org/10.1111/GCB.12583.

Colombaroli, D., van der Plas, G., Rucina, S., Verschuren, D., 2018. Determinants of savanna-fire dynamics in the eastern Lake Victoria catchment (western Kenya) during the last 1200 years. Quat. Int. 488, 67–80. https://doi.org/10.1016/J.QUAINT.2016.06.028.

Conedera, M., Tinner, W., Neff, C., Meurer, M., Dickens, A.F., Krebs, P., 2009. Reconstructing past fire regimes: methods, applications, and relevance to fire management and conservation. Quat. Sci. Rev. 28 (5–6), 555–576.

Damsté, J.S.S., Ossebaar, J., Schouten, S., Verschuren, D., 2012. Distribution of tetraether lipids in the 25-ka sedimentary record of Lake Challa: extracting reliable TEX86 and MBT/CBT palaeotemperatures from an equatorial African lake. Quaternary Science Reviews 50, 43–54.

Demenocal, P., Ortiz, J., Guilderson, T., Adkins, J., Sarnthein, M., Baker, L., Yarusinsky, M., 2000. Abrupt onset and termination of the African Humid Period:: rapid climate responses to gradual insolation forcing. Quat. Sci. Rev. 19 (1–5), 347–361.

Desmedt, C., 1991. Poteries anciennes décorées à la roulette dans la Région des Grands Lacs. Afr. Archaeol. Rev. 9 (1), 161–196. https://doi.org/10.1007/BF01117220, 1991 9:1.

Duane, W.J., Pepin, N.C., Losleben, M.L., Hardy, D.R., 2008. General characteristics of temperature and humidity variability on Kilimanjaro, Tanzania. Arctic Antarct. Alpine Res. 40 (2), 323–334. https://doi.org/10.1657/1523-0430(06-127[DUANE]2.0.CO;2.

Erdman, C., Emerson, J.W., 2007. Bcp: an R package for performing a bayesian analysis of change point problems. J. Stat. Software 23 (3), 1–13.

Garcin, Y., Vincens, A., Williamson, D., Buchet, G., Guiot, J., 2007. Abrupt resumption of the African monsoon at the younger dryas—holocene climatic transition. Quat. Sci. Rev. 26 (5–6), 690–704. https://doi.org/10.1016/j.quascirev.2006.10.014.

Gasse, F., 2000. Hydrological changes in the African tropics since the last glacial maximum. Quat. Sci. Rev. 19 (1–5), 189–211. https://doi.org/10.1016/S0277-3791(99)00061-X.

Genet, M., Daniau, A.L., Mouillot, F., Hanquiez, V., Schmidt, S., David, V., et al., 2021. Modern relationships between microscopic charcoal in marine sediments and fire regimes on adjacent landmasses to refine the interpretation of marine paleofire records: an Iberian case study. Quat. Sci. Rev. 270, 107148.

Gillson, L., 2004. Testing non-equilibrium theories in savannas: 1400 years of vegetation change in Tsavo National Park, Kenya. Ecol. Complex. 1 (4), 281–298.

Githumbi, E.N., 2017. Holocene Environmental and Human Interactions in East Africa. Doctoral dissertation, University of York.

Goldstein, S.T., Munyiri, J.M., 2017. The elmenteitan obsidian quarry (GsJj50): new perspectives on obsidian access and exchange during the pastoral neolithic in southern Kenya. Afr. Archaeol. Rev. 34 (1), 43–73. https://doi.org/10.1007/S10437-016-9240-0/TABLES/4.

Gosling, W.D., Miller, C.S., Livingstone, D.A., 2013. Atlas of the tropical West African pollen flora. Rev. Palaeobot. Palynol. 199, 1–135. https://doi.org/10.1016/J.REVPALBO.2013.01.003.

Hamilton, S., Munyaho, A.T., Krach, N., Glaser, S., 2016. Lake Victoria Bathymetry Contours, V7.

Hemp, A., 2005. Climate change-driven forest fires marginalize the impact of ice cap wasting on Kilimanjaro. Global Change Biol. 11, 1013–1023.

Hemp, A., Beck, E., 2001. Erica excelsa as a fire-tolerating component of Mt. Kilimanjaro's forests. Phytocoenologia 31, 449–475.

Henne, P.D., Elkin, C., Franke, J., Colombaroli, D., Calò, C., La Mantia, T., et al., 2015. Reviving extinct Mediterranean forest communities may improve ecosystem potential in a warmer future. Front. Ecol. Environ. 13 (7), 356–362.

Huffman, T.N., 1982. Archaeology and ethnohistory of the African iron age. Annu. Rev. Anthropol. 11 (1), 133–150.

Humphris, J., Iles, L., 2013. Pre-colonial iron production in great lakes Africa: recent research at UCL Institute of Archaeology. World Iron 56–65.

Iles, L., Lane, P., 2015. Iron production in second millennium AD pastoralist contexts on the Laikipia Plateau, Kenya. Azania 50 (3), 372–401.
Ivory, S.J., Russell, J., 2016. Climate, herbivory, and fire controls on tropical African forest for the last 60ka. Quat. Sci. Rev. 148, 101–114. https://doi.org/10.1016/j.quascirev.2016.07.015.
Johnson, T.C., Scholz, C.A., Talbot, M.R., Kelts, K., Ricketts, R.D., Ngobi, G., Beuning, K.R.M., Ssemmanda, I., McGill, J.W., 1996. Late Pleistocene desiccation of Lake Victoria and rapid evolution of cichlid fishes. Science 273 (5278), 1091–1093.
Johnson, T.C., Chan, Y., Beuning, K., Kelts, K., Ngobi, G., Verschuren, D., 1998. Biogenic silica profiles in Holocene cores from Lake Victoria: implications for lake level history and initiation of the Victoria Nile. In: Environmental Change and Response in East African Lakes. Springer, Dordrecht, pp. 75–88.
Kendall, R.L., 1969. An ecological history of the Lake Victoria basin. Ecol. Monogr. 39 (2), 121–176.
Kindt, R., van Breugel, P., Orwa, C., Lillesø, J.P.B., Jamnadass, R., Graudal, L., 2015. Useful Tree Species for Eastern Africa: a Species Selection Tool Based on the VECEA Map.
Köppen, W., 1936. Das geographische system der Klimate. In: Köppen, W., Geiger, R. (Eds.), Handbuck der Klimatologie Bd. 1, Teil C. Gebrüder Bornträger, Berlin.
Lamb, H.F., Bates, C.R., Coombes, P.V., Marshall, M.H., Umer, M., Davies, S.J., Dejen, E., 2007. Late Pleistocene desiccation of Lake Tana, source of the blue nile. Quat. Sci. Rev. 26 (3–4), 287–299. https://doi.org/10.1016/j.quascirev.2006.11.020.
Long, C.J., Whitlock, C., Bartlein, P.J., Millspaugh, S.H., 1998. A 9000-year Fire History from the Oregon Coast Range, Based on a High-Resolution Charcoal Study.
Loomis, S.E., Russell, J.M., Verschuren, D., Morrill, C., De Cort, G., Sinninghe Damsté, J.S., et al., 2017. The tropical lapse rate steepened during the Last Glacial Maximum. Sci. Adv. 3 (1), e1600815.
Marchant, R., 2021. East Africa's human environment interactions. In: East Africa's Human Environment Interactions. Palgrave Macmillan, pp. 39–114. https://doi.org/10.1007/978-3-030-88987-6_2.
Marchant, R., Mumbi, C., Behera, S., Yamagata, T., 2007. The Indian Ocean dipole—the unsung driver of climatic variability in East Africa. Afr. J. Ecol. 45 (1), 4–16.
Marchant, R., Richer, S., Boles, O., Capitani, C., Courtney-Mustaphi, C.J., Lane, P., et al., 2018. Drivers and trajectories of land cover change in East Africa: human and environmental interactions from 6000 years ago to present. Earth Sci. Rev. 178, 322–378.
Marlon, J.R., 2020. What the past can say about the present and future of fire. Quat. Res. 96, 66–87. https://doi.org/10.1017/qua.2020.48.
Millspaugh, S.H., Whitlock, C., 1995. A 750-year fire history based on lake sediment records in central Yellowstone National Park, USA. Holocene 5 (3), 283–292.
Mooney, S.D., Tinner, W., 2011. The analysis of charcoal in peat and organic sediments. Mires Peat 7 (9), 1–18.
Moore, P., Webb, J.A., Collinson, M.E., 1991. Pollen Analysis, Second. Blackwell Scientific Publications.
Mustaphi, C.J.C., Kinyanjui, R., Shoemaker, A., Mumbi, C., Muiruri, V., Marchant, L., et al., 2021. A 3000-year record of vegetation changes and fire at a high-elevation wetland on Kilimanjaro, Tanzania. Quat. Res. 99, 34–62.
M'Mbogori, F.N., 2021. Human and environmental interactions in late iron age Kenya. In: Oxford Research Encyclopedia of Anthropology.
Nakintu, J., Lejju, J., 2016. Environmental dynamics of Lake Victoria: evidence from a 10,000 14C yr diatom record from napoleon gulf and sango Bay. J. Environ. Sci. Eng. 5, 626–637.
Nelson, D.M., Verschuren, D., Urban, M.A., Hu, F.S., 2012. Long-term variability and rainfall control of savanna fire regimes in equatorial East Africa. Global Change Biol. 18 (10), 3160–3170. https://doi.org/10.1111/j.1365-2486.2012.02766.x.
Nicholson, S.E., 2018. The ITCZ and the seasonal cycle over equatorial Africa. Bull. Am. Meteorol. Soc. 99 (2), 337–348. https://doi.org/10.1175/BAMS-D-16-0287.1.
Nyamweya, C., Desjardins, C., Sigurdsson, S., Tomasson, T., Taabu-Munyaho, A., Sitoki, L., Stefansson, G., 2016. Simulation of Lake Victoria circulation patterns using the regional ocean modeling system (ROMS). PLoS One 11 (3), e0151272.
Okungu, J., Njoka, S., Abuodha, J.O.Z., Hecky, R.E., 2005. Lake Victoria Environment Report Water Quality and Ecosystem Status: Kenya National Water Quality Synthesis Report.
Olsson, I.U., 2009. Radiocarbon dating history: early days, questions, and problems met. Radiocarbon 51 (1), 1–43.
Pedrotta, T., Gobet, E., Schwörer, C., Beffa, G., Butz, C., Henne, P.D., et al., 2021. 8,000 years of climate, vegetation, fire and land-use dynamics in the thermo-mediterranean vegetation belt of northern Sardinia (Italy). Veg. Hist. Archaeobotany 30 (6), 789–813.
Power, M.J., Marlon, J., Ortiz, N., Bartlein, P.J., Harrison, S.P., Mayle, F.E., et al., 2008. Changes in fire regimes since the Last Glacial Maximum: an assessment based on a global synthesis and analysis of charcoal data. Clim. Dynam. 30 (7), 887–907.
Reille, M., 1992. Pollen et spores d'Europe et d'Afrique du nord. Laboratoire de Botanique Historique et Palynologie.
Reimer, P.J., William, •, Austin, E.N., Bard, • Edouard, Bayliss, A., Paul, •, Blackwell, G., Christopher, •, Ramsey, B., Butzin, M., Cheng, H., Lawrence Edwards, • R., Friedrich, • Michael, Pieter, •, Grootes, M., Thomas, •, Guilderson, P., Hajdas, I., Heaton, T.J., et al., 2020. Chronos 14 carbon-cycle facility, the changing earth research centre, and school of biological. Earth Environ. Sci. 62, 23. https://doi.org/10.1017/RDC.2020.41.
Roubik, D.W., Moreno, P.J.E., 1991. Pollen and Spores of Barro Colorado Island ([Panama]).
Rucina, S.M., Muiruri, V.M., Kinyanjui, R.N., McGuiness, K., Marchant, R., 2009. Late Quaternary vegetation and fire dynamics on Mount Kenya. Palaeogeogr. Palaeoclimatol. Palaeoecol. 283 (1–2), 1–14. https://doi.org/10.1016/j.palaeo.2009.08.008.
Salazar, G., Zhang, Y.L., Agrios, K., Szidat, S., 2015. Development of a method for fast and automatic radiocarbon measurement of aerosol samples by online coupling of an elemental analyzer with a MICADAS AMS. Nucl. Instrum. Methods Phys. Res. Sect. B Beam Interact. Mater. Atoms 361, 163–167.
Schoenbrun, D.L., 1993. We are what we eat: ancient agriculture between the great lakes. J. Afr. Hist. 34 (1), 1–31.
Schoenbrun, D.L., 1998. A Green Place, a Good Place: Agrarian Change, Gender, and Social Identity in the Great Lakes Region to the 15th Century. Heinemann, Portsmouth.
Schüler, L., Hemp, A., 2016. Atlas of pollen and spores and their parent taxa of Mt Kilimanjaro and tropical East Africa. Quat. Int. 425, 301–386. https://doi.org/10.1016/J.QUAINT.2016.07.038.
Schüler, L., Hemp, A., Zech, W., Behling, H., 2012. Vegetation, climate and fire-dynamics in East Africa inferred from the Maundi crater pollen record from Mt Kilimanjaro during the last glacial-interglacial cycle. Quat. Sci. Rev. 39, 1–13. https://doi.org/10.1016/j.quascirev.2012.02.003.
Stager, J.C., 1984. The diatom record of Lake Victoria (East Africa): the last 17,000 years. Proceed. Seventh Int. Diatom Symp. 455–476.
Stager, J.C., Cumming, B., Meeker, L., 1997. A high-resolution 11,400-yr diatom record from Lake Victoria, East Africa. Quat. Res. 47 (1), 81–89. https://doi.org/10.1006/qres.1996.1863.
Stager, J.C., Johnson, T.C., 2000. A 12,400 14C yr offshore diatom record from east central Lake Victoria, East Africa. J. Paleolimnol. 23 (4), 373–383.
Stager, J.C., Reinthal, P.N., Livingstone, D.A., 1986. A 25,000-year history for Lake Victoria, East Africa, and some comments on its significance for the evolution of cichlid fishes. Freshw. Biol. 16 (1), 15–19. https://doi.org/10.1111/j.1365-2427.1986.tb00944.x.
Stager, J.C., Ryves, D.B., Chase, B.M., Pausata, F.S.R., 2011. Catastrophic drought in the Afro-Asian monsoon region during Heinrich event 1. Science 331 (6022), 1299–1302. https://doi.org/10.1126/science.1198322.
Stockmarr, J., 1971. Tablets with spores used in absolute pollen analysis. Pollen Spores 13, 615–621.
Stuiver, M., 1970. Oxygen and carbon isotope ratios of fresh-water carbonates as climatic indicators. J. Geophys. Res. 75 (27), 5247–5257.
Stuiver, M., Polach, H.A., 1977. Discussion reporting of 14C data. Radiocarbon 19 (3), 355–363.
Szidat, S., Salazar, G.A., Vogel, E., Battaglia, M., Wacker, L., Synal, H.A., Türler, A., 2014. 14C analysis and sample preparation at the new Bern Laboratory for the Analysis of Radiocarbon with AMS (LARA). Radiocarbon 56 (2), 561–566.
Talbot, M.R., Filippi, M.L., Jensen, N.B., Tiercelin, J.-J., 2007. An abrupt change in the African monsoon at the end of the Younger Dryas. G-cubed 8 (3), 1–16. https://doi.org/10.1029/2006GC001465.
Talbot, M.R., Lærdal, T., 2000. The Late Pleistocene-Holocene palaeolimnology of Lake Victoria, East Africa, based upon elemental and isotopic analyses of sedimentary organic matter. Journal of Paleolimnology 23 (2), 141–164.
ter Braak, C.J.F., Prentice, I.C., 1988. A theory of gradient analysis. In: Begon, M., Fitter, A.H., Ford, E.D., Macfadyen, A. (Eds.), Advances in Ecological Research. Academic Press, pp. 271–317.
ter Braak, C.J.F., Šmilauer, P., 2018. Canoco Reference Manual and User's Guide: Software for Ordination (5.10. Biometris.
Thevenon, F., Williamson, D., Vincens, A., Taieb, M., Merdaci, O., Decobert, M., Buchet, G., 2003. A late-Holocene charcoal record from Lake Masoko, SW Tanzania: climatic and anthropologic implications. Holocene 13 (5), 785–792. https://doi.org/10.1191/0959683603hl665rr.
Tierney, J.E., Russell, J.M., Huang, Y., Damsté, J.S.S., Hopmans, E.C., Cohen, A.S., 2008. Northern hemisphere controls on tropical southeast African climate during the past 60,000 years. Science 322 (5899), 252–255.
Vincens, A., Buchet, G., Williamson, D., Taieb, M., 2005. A 23,000 yr pollen record from Lake Rukwa (8°S, SW Tanzania): new data on vegetation dynamics and climate in Central Eastern Africa. Rev. Palaeobot. Palynol. 137 (3–4), 147–162. https://doi.org/10.1016/j.revpalbo.2005.06.001.
Walker, M., 2005. Quaternary Dating Methods. John Wiley and Sons.
White, 1983. The Vegetation of Africa. A Descriptive Memoir to Accompany the Unesco/AETFAT/UNSO Vegetation Map of Africa, UNESCO.
Whitlock, C., Higuera, P.E., McWethy, D.B., Briles, C.E., 2010. Paleoecological perspectives on fire ecology: revisiting the fire-regime concept. Open Ecol. J. 3 (1).
Wirrmann, D., Bertaux, J., Kossoni, A., 2001. Late Holocene paleoclimatic changes in western central Africa inferred from mineral abundance in dated sediments from Lake ossa (southwest Cameroon). Quat. Res. 56 (2), 275–287. https://doi.org/10.1006/qres.2001.2240.
Zander, P.D., Szidat, S., Kaufman, D.S., Żarczyński, M., Poraj-Górska, A.I., Boltshauser-Kaltenrieder, P., Grosjean, M., 2020. Miniature radiocarbon measurements (< 150 μg C) from sediments of Lake Żabińskie, Poland: effect of precision and dating density on age–depth models. Geochronology 2 (1), 63–79.
Zhao, Y., Yu, Z., 2012. Vegetation response to Holocene climate change in East Asian monsoon-margin region. Earth Sci. Rev. 113 (1–2), 1–10. https://doi.org/10.1016/j.earscirev.2012.03.001.